

## Ocean community warming responses explained by thermal affinities and temperature gradients

Burrows, Michael T.; Bates, Amande E.; Costello, Mark J.; Edwards, Martin; Edgar, Graham J.; Fox, Clive J.; Halpern, B.S.; Hiddink, Jan Geert; Pinsky, M.L.; Batt, Ryan D.; Molinos, J.G.; Payne, Ben; Schoeman, David; Stuart-Smith, Rick D.; Poloczanska, E.S.

### Nature Climate Change

DOI:

[10.1038/s41558-019-0631-5](https://doi.org/10.1038/s41558-019-0631-5)

Published: 25/11/2019

Peer reviewed version

[Cyswllt i'r cyhoeddiad / Link to publication](#)

*Dyfyniad o'r fersiwn a gyhoeddwyd / Citation for published version (APA):*

Burrows, M. T., Bates, A. E., Costello, M. J., Edwards, M., Edgar, G. J., Fox, C. J., Halpern, B. S., Hiddink, J. G., Pinsky, M. L., Batt, R. D., Molinos, J. G., Payne, B., Schoeman, D., Stuart-Smith, R. D., & Poloczanska, E. S. (2019). Ocean community warming responses explained by thermal affinities and temperature gradients. *Nature Climate Change*, 9(12), 959-963. <https://doi.org/10.1038/s41558-019-0631-5>

#### Hawliau Cyffredinol / General rights

Copyright and moral rights for the publications made accessible in the public portal are retained by the authors and/or other copyright owners and it is a condition of accessing publications that users recognise and abide by the legal requirements associated with these rights.

- Users may download and print one copy of any publication from the public portal for the purpose of private study or research.
- You may not further distribute the material or use it for any profit-making activity or commercial gain
- You may freely distribute the URL identifying the publication in the public portal ?

#### Take down policy

If you believe that this document breaches copyright please contact us providing details, and we will remove access to the work immediately and investigate your claim.

**Ocean community warming responses explained by thermal affinities and temperature gradients**

Michael T. Burrows<sup>1\*</sup>, Amanda E. Bates<sup>2,3</sup>, Mark J. Costello<sup>4</sup>, Martin Edwards<sup>5,6</sup>,  
Graham J. Edgar<sup>7</sup>, Clive J. Fox<sup>1</sup>, Benjamin S. Halpern<sup>8,9,10</sup>, Jan G. Hiddink<sup>11</sup>, Malin L. Pinsky<sup>12</sup>,  
Ryan D. Batt<sup>12</sup>, Jorge García Molinos<sup>13,14</sup>, Ben Payne<sup>1</sup>, David Schoeman<sup>15,16</sup>, Rick D. Stuart-Smith<sup>7</sup>, Elvira S. Poloczanska<sup>17,18</sup>

**As ocean temperatures rise, species distributions are tracking towards historically cooler regions in line with their thermal affinity<sup>1,2</sup>. However, warming, different species responses and presence of other species means predicting biodiversity redistribution and relative abundance remains a challenge <sup>3,4</sup>. Here we use three decades of fish and plankton survey data to assess how warming changes the relative dominance of warm-affinity and cold-affinity species<sup>5,6</sup>. Regions with stable temperatures show little change in dominance structure (Northeast Pacific, Gulf of Mexico), while warming sees strong shifts towards warm-water species dominance (North Atlantic). Importantly, communities whose species pools had diverse thermal affinities and narrower range of thermal tolerance show greater sensitivity, as anticipated from simulations. Composition of fish communities changed less than expected in regions with strong temperature depth gradients. There, species track temperatures by moving deeper<sup>2,7</sup>, rather than horizontally, analogous to elevation shifts in land plants<sup>8</sup>. Temperature thus emerges as a fundamental driver for change in marine systems, with predictable restructuring of communities in the most rapidly warming areas using metrics based on species thermal affinities derived for diverse taxa. The emerging relationships provide a metric for assessment of biodiversity model predictions. The ready**

**and predictable dominance shifts suggests a strong prognosis of resilience to climate change for these communities.**

Abundance and distributions of marine species are changing in response to anthropogenic climate change<sup>1</sup> but these changes vary geographically and across taxa. Shifts in geographical range and temporal species turnover, for example, tend to be accelerated where temperature changes coincide with widely spaced isotherms<sup>1,2</sup>. Unlike terrestrial ecosystems, marine species may be unable to shelter from extreme temperatures, making the effect of ambient temperature immediate, unavoidable, and easier to detect. Local gain and loss of species, combined with changes in the relative abundance of species with different thermal affinities, drive change in community structure. On land, failure of species distributions to track temperature means that community thermal composition lags behind expected change, seen in communities of birds, butterflies, and plant species<sup>5,9-14</sup>. Identifying the aspects of community change that can be accurately forecasted is needed to assist managers to adaptively deal with ecosystem change.

We use time series of species incidence in standardised international surveys of plankton and demersal species since 1985 (Supplementary Table 1) to quantify regional changes in community structure. Combined with estimates of species' thermal affinities, these data describe regional changes in the average thermal affinity of marine communities, as measured by the Community Temperature Index (CTI, Supplementary Table 2). CTI is the community-wide average of species' thermal affinities, which are calculated from each Species Temperature Index, STI (the median of sea surface temperatures across each species' estimated geographical range, see Methods and Fig. 1a). The variation of thermal affinities among species (Community Thermal Diversity, CTDiv) is here described by the incidence-weighted standard deviation of STIs. Low values of thermal diversity reflect communities composed of species with similar

STIs, and high values reflect communities composed of a mix of warm- and cold-water species. The incidence-weighted average width of species' thermal ranges (STRs, Fig. 1a), the Community Thermal Range (CTR), indicates whether communities are composed of broad-ranged species (eurytherms) or narrow-ranged species (stenotherms). The fact that distributions of marine ectotherms generally fill their thermal tolerances<sup>15</sup> supports the inference that thermal range can be approximated by species' geographic range.

The difference between CTI and local temperature (used to define STIs) is termed community thermal bias: positive where communities are dominated by species from warmer areas, implying reduced sensitivity to warming<sup>16</sup>, and negative for communities dominated by species from colder areas, implying increased vulnerability<sup>17</sup>. Less compositional change in response to temperature is expected in areas of strong vertical and horizontal gradients in ocean temperature (and low velocity of climate change<sup>18</sup>) because small shifts may allow species to remain in the same temperature as before. Thermal bias is distinct from CTI lag<sup>5</sup> or extinction debt, since it refers to the difference in spatial patterns of temperature and average thermal affinity rather than to a perceived delay in community response to temperature change.

We focused on the sensitivity of CTI to regional temperature change (sCTI), defined as the ratio of the change in CTI through time to the corresponding change in environmental temperature. We evaluated the influence of community thermal diversity and community thermal range on CTI sensitivity by developing quantitative expectations from simulations. These simulated communities comprised pools of species with a thermal diversity set by the standard deviation of STI values. Each species had incidence-temperature curves<sup>19</sup> defined by their thermal range (Gaussian Fig. 1a, other forms in Supplementary Fig. 1), consistent with organisms more abundant near the middle of their range<sup>20,21</sup>. While contested<sup>22</sup>, the Gaussian

pattern holds for our fish and plankton datasets (Fig. 1b, Supplementary Fig. 3) when abundance and incidence data are expressed relative to thermal range location. We used species' thermal ranges and temperature changes to simulate changes in species incidence with temperature which, when aggregated across species, produced changes in CTI. Simulated CTI sensitivity was large where thermally diverse communities were made up of narrow-ranged species<sup>17</sup> (Fig. 1c, g), but smaller where thermal ranges were broad or thermal diversity was low (Fig. 1d, f, g). For functions with declining abundance from a central maximum, simulated CTI sensitivity suggested more change in thermally diverse communities made up of small-ranged species, and less in communities of species with similar thermal affinities and large thermal ranges (Supplementary Fig. 2, Supplementary Table 4). With Gaussian curves, CTI sensitivity was proportional to the squared ratio of thermal diversity to average range width (Fig 1g and Supplementary Table 2), independent of thermal bias (see also <sup>23</sup>). Below we explored this hypothesized relationship with empirical data.

Spatial patterns in CTI for demersal species and plankton, averaged from 1985 to 2014, broadly followed patterns in surface temperatures in the HadISST1 dataset<sup>24</sup> and seabed temperatures from the Hadley Centre EN4 dataset<sup>25</sup> (Supplementary Figs. 5a, 9a). Community thermal diversity was highest midway along thermal gradients. Thermal ranges were larger for plankton than demersal species, with plankton thermal ranges increasing in size with latitude (Supplementary Figs. 5b, 6). Average species' thermal affinity and range width in 2° grid cells were positively correlated in cool-temperate latitudes, where cold-affinity species having smaller thermal ranges than those from lower latitudes, and negatively correlated towards sub-tropical areas (Supplementary Fig. 6d). This pattern results from the bounds on species thermal ranges at the equator and the poles (Supplementary Figs 5, 6).

For SST-derived CTIs, areas with strong vertical temperature gradients had more negative community thermal bias in demersal species (Fig. 3a), with species' STIs more associated with cooler subsurface (50-100 m) rather than surface temperature. Plankton community thermal bias was less influenced by vertical gradients, suggesting a stronger association with surface temperatures. CTI derived from seabed temperature was more weakly associated with the spatial pattern in SBT (Methods, Supplementary Fig. 9g).

Both plankton and demersal communities, aggregated over 2° areas, changed in thermal affinity from 1985 to 2014 (Fig. 2, Supplementary Fig. 8) at local (<500 km) to ocean-basin scales (10,000 km). Sea surface temperatures warmed across the North Atlantic over this period by up to 0.5°C per decade, but cooled slightly or stayed the same in the Northeast Pacific (Fig. 2a,b). Regional trends in CTI for plankton and for demersal fish and invertebrates more clearly followed trends in sea surface temperature ( $R^2 = 0.23$ , Fig. 2e) than seabed temperature ( $R^2 = 0.1$  Supplementary Fig. 9g). Demersal communities shifted towards dominance by warm-water species around northeast USA and Europe, while North Pacific, southeast USA and other areas with little temperature change had stable CTIs (Fig. 2c). CTI changes in plankton communities were also most pronounced in areas of greater SST change in the northwest Atlantic and the northwest European Shelf (Fig. 2d).

In European waters, CTI for demersal species changed more consistently than plankton CTI (Fig. 2c,d), especially in the southern North Sea, despite observed large distribution changes in plankton species<sup>26</sup>. Reduced CTI sensitivity in plankton is expected given the greater temperature ranges of plankton species compared to demersal invertebrates and fishes (Supplementary Figs 5c, 6d). The positive effect of thermal diversity and inverse effect of community thermal range (CTR) on CTI sensitivity explained much of the variability in

responses of community composition to warming ( $R^2=0.39$ ), but the negative and near-zero response of Canadian demersal communities remained (Fig. 3c). Vertical gradients in temperature (up to 7°C over the top 50m) explained much of the remaining variation in sensitivity of CTI to temperature, improving the performance of regression models (Fig. 3c, Supplementary Table 4). SST-derived thermal bias in natural communities had a small positive effect on sensitivity, but this effect was lost when compared alongside vertical and horizontal gradients in regression models (Supplementary Table 4, Model R1). Horizontal spatial gradients in surface temperature had no effect on CTI sensitivity when considered with vertical gradients (Supplementary Table 4).

Reduced CTI sensitivity to surface warming in areas of steep vertical temperature gradients is consistent with a redistribution of species to greater depths<sup>27</sup>. Such vertical gradients may allow thermal niche tracking without horizontal shifts, and may provide refugia for cold-water species without significant ecological consequences, unless limited to the surface by a need for light (phytoplankton, coral, macroalgae), or habitat (intertidal organisms). The lack of influence of horizontal thermal gradients on CTI sensitivity to surface temperature change suggests that horizontal shifts in species distribution had comparatively little effect at the scale of the analysis ( $2^\circ \times 2^\circ$  grids over 30 years).

Patterns of observed CTI sensitivity matched expectations from simulations. More change in community composition was seen in communities composed of species with greater diversity of thermal affinities, narrower thermal ranges, and without access to refuges from climate change at greater depths (i.e., outside areas of steep vertical temperature gradients where observed changes do not match predictions). While negative thermal bias has been implicated as an indicator for community-level vulnerability with warming<sup>17</sup>, we found instead instances of apparent negative

SST-derived thermal bias (e.g. demersal species in the Canadian Atlantic Maritimes: Fig. 3a) that were better explained by vertical temperature gradients, with species' affinities closer to temperatures experienced at depth than surface temperatures.

Studies of birds, butterflies and plant communities showing smaller changes in CTI than changes in temperature have generally been interpreted as lags in response<sup>5,9-12</sup>, but thermal range width and community thermal range effects on CTI sensitivity may explain some of these apparent lags. Short-lived plankton and species of highly mobile fish and invertebrates may be more responsive to temperature change in time and space<sup>2,6</sup> than analogous communities on land, potentially as a consequence of living closer to their thermal limits<sup>28</sup>. Communities of long-lived, slowly dispersing species may be less responsive in thermal affinity composition when increasing in abundance, but may decline rapidly, as in the loss of cold-water kelp and influx of tropical fish in response to a recent warming event in Western Australia<sup>29</sup>. Slower-than-expected community responses may also be caused by compensatory population dynamics<sup>30</sup> in individual species. Replacement of cooler-affinity species by incoming warmer-affinity species is not possible in the tropics, likely resulting in the depression in species richness at the equator<sup>31</sup>. In addition, geographical barriers can also restrict routes for incoming migrants, such as in the Mediterranean<sup>32</sup>, resulting in a lowered species turnover<sup>6</sup> and capacity for CTI change<sup>17</sup>.

Our study shows the dominant effects of recent temperature change on community turnover across marine species from regional to ocean scales, regardless of other influences such as fishing impacts and ocean acidification. The prediction of temperature effects at community scales derived from species thermal performance curves<sup>33</sup> provides a benchmark against which the pace of reorganization of global biodiversity to climate can be judged, and allows assessment of the performance of quantitative models<sup>3,4</sup>. The predictability with which thermal diversity,



average thermal range width and vertical temperature gradients directly drive patterns of sensitivity of community composition to warming gives a strong prognosis for the resilience of ocean communities to respond to climate change. In the northern temperate coastal oceans in this study, warm-tolerant species of plankton and fishes are slowly replacing their cold-tolerant counterparts over the timescales of climate change, and if those species have similar roles, suggesting a capacity for the oceans to continue to function.

## References

- 1 Poloczanska, E. S. *et al.* Global imprint of climate change on marine life. *Nature Climate Change* **3**, 919-925, doi:10.1038/nclimate1958 (2013).
- 2 Pinsky, M. L., Worm, B., Fogarty, M. J., Sarmiento, J. L. & Levin, S. A. Marine taxa track local climate velocities. *Science* **341**, 1239-1242, doi:10.1126/science.1239352 (2013).
- 3 Jones, M. C. & Cheung, W. W. L. Multi-model ensemble projections of climate change effects on global marine biodiversity. *ICES Journal of Marine Science: Journal du Conseil* **72**, 741-752, doi:10.1093/icesjms/fsu172 (2015).
- 4 García Molinos, J. *et al.* Climate velocity and the future global redistribution of marine biodiversity. *Nature Climate Change* **6**, 83, doi:10.1038/nclimate2769 (2016).
- 5 Devictor, V. *et al.* Differences in the climatic debts of birds and butterflies at a continental scale. *Nature Climate Change* **2**, 121, doi:10.1038/nclimate1347 (2012).
- 6 Cheung, W. W. L., Watson, R. & Pauly, D. Signature of ocean warming in global fisheries catch. *Nature* **497**, 365-368, doi:10.1038/nature12156 (2013).
- 7 Perry, A. L., Low, P. J., Ellis, J. R. & Reynolds, J. D. Climate change and distribution shifts in marine fishes. *Science* **308**, 1912-1912 (2005).
- 8 Lenoir, J., Gégout, J. C., Marquet, P. A., de Ruffray, P. & Brisse, H. A significant upward shift in plant species optimum elevation during the 20th century. *Science* **320**, 1768 (2008).
- 9 Lindström, Å., Green, M., Paulson, G., Smith, H. G. & Devictor, V. Rapid changes in bird community composition at multiple temporal and spatial scales in response to recent climate change. *Ecography* **36**, 313, doi:10.1111/j.1600-0587.2012.07799.x (2013).
- 10 Nieto-Sánchez, S., Gutiérrez, D. & Wilson, R. J. Long-term change and spatial variation in butterfly communities over an elevational gradient: driven by climate, buffered by habitat. *Divers. Distrib.* **21**, 950, doi:10.1111/ddi.12316 (2015).
- 11 Santangeli, A., Rajasärkkä, A. & Lehtikoinen, A. Effects of high latitude protected areas on bird communities under rapid climate change. *Glob. Change Biol.* **23**, 2241-2249 (2017).
- 12 Bertrand, R. *et al.* Changes in plant community composition lag behind climate warming in lowland forests. *Nature* **479**, 517, doi:10.1038/nature10548 (2011).
- 13 De Frenne, P. *et al.* Microclimate moderates plant responses to macroclimate warming. *Proceedings of the National Academy of Sciences* **110**, 18561-18565 (2013).

- 201 14 Flanagan, P. H., Jensen, O. P., Morley, J. W. & Pinsky, M. L. Response of marine  
202 communities to local temperature changes. *Ecography* (2018).
- 203 15 Sunday, J. M., Bates, A. E. & Dulvy, N. K. Thermal tolerance and the global redistribution  
204 of animals. *Nature Climate Change* **2**, 686-690, doi:10.1038/nclimate1539 (2012).
- 205 16 Deutsch, C. A. *et al.* Impacts of climate warming on terrestrial ectotherms across latitude.  
206 *Proceedings of the National Academy of Sciences* **105**, 6668-6668 (2008).
- 207 17 Stuart-Smith, R. D., Edgar, G. J., Barrett, N. S., Kininmonth, S. J. & Bates, A. E. Thermal  
208 biases and vulnerability to warming in the world's marine fauna. *Nature* **528**, 88-92,  
209 doi:10.1038/nature16144 (2015).
- 210 18 Burrows, M. T. *et al.* The pace of shifting climate in marine and terrestrial ecosystems.  
211 *Science* **334**, 652-655, doi:10.1126/science.1210288 (2011).
- 212 19 Beaugrand, G. Theoretical basis for predicting climate-induced abrupt shifts in the oceans.  
213 *Philosophical Transactions of the Royal Society B: Biological Sciences* **370**, 20130264,  
214 doi:10.1098/rstb.2013.0264 (2015).
- 215 20 Brown, J. H. On the relationship between abundance and distribution of species. *Am. Nat.*  
216 **124**, 255–279 (1984).
- 217 21 Waldock, C., Stuart - Smith, R. D., Edgar, G. J., Bird, T. J. & Bates, A. E. The shape of  
218 abundance distributions across temperature gradients in reef fishes. *Ecol. Lett.* **22**, 685-696  
219 (2019).
- 220 22 Sagarin, R. D. & Gaines, S. D. The 'abundant centre' distribution: to what extent is it a  
221 biogeographical rule? *Ecol. Lett.* **5**, 137-147 (2002).
- 222 23 Bonachela, J. A., Burrows, M. T., Payne, M. R. & Pinsky, M. L. Rate of community  
223 response to climate change depends on species traits and community composition. *Am. Nat.*  
224 **in review** (2019).
- 225 24 Rayner, N. A. *et al.* Global analyses of sea surface temperature, sea ice, and night marine air  
226 temperature since the late nineteenth century. *J. Geophys. Res* **108**, 4407-4407 (2003).
- 227 25 Good, S. A., Martin, M. J. & Rayner, N. A. EN4: Quality controlled ocean temperature and  
228 salinity profiles and monthly objective analyses with uncertainty estimates. *Journal of*  
229 *Geophysical Research: Oceans* **118**, 6704-6716 (2013).
- 230 26 Beaugrand, G., Luczak, C. & Edwards, M. Rapid biogeographical plankton shifts in the  
231 North Atlantic Ocean. *Glob. Change Biol.* **15**, 1790-1803 (2009).
- 232 27 Dulvy, N. K. *et al.* Climate change and deepening of the North Sea fish assemblage: a biotic  
233 indicator of warming seas. *J. Appl. Ecol.* **45**, 1029–1039-1029–1039 (2008).
- 234 28 Pinsky, M. L., Eikeset, A. M., McCauley, D. J., Payne, J. L. & Sunday, J. M. Greater  
235 vulnerability to warming of marine versus terrestrial ectotherms. *Nature* **569**, 108 (2019).
- 236 29 Wernberg, T. *et al.* An extreme climatic event alters marine ecosystem structure in a global  
237 biodiversity hotspot. *Nature Climate Change* **3**, 78-82, doi:10.1038/nclimate1627 (2013).
- 238 30 Doak, D. F. & Morris, W. F. Demographic compensation and tipping points in climate-  
239 induced range shifts. *Nature* **467**, 959, doi:10.1038/nature09439 (2010).
- 240 31 Chaudhary, C., Saeedi, H. & Costello, M. J. Bimodality of latitudinal gradients in marine  
241 species richness. *Trends Ecol. Evol.* **31**, 670-676 (2016).
- 242 32 Burrows, M. T. *et al.* Geographical limits to species-range shifts are suggested by climate  
243 velocity. *Nature* **507**, 492, doi:10.1038/nature12976 (2014).
- 244 33 Pörtner, H. O. & Farrell, A. P. Physiology and climate change. *Science* **322**, 690 (2008).

- 34 Kramer - Schadt, S. *et al.* The importance of correcting for sampling bias in MaxEnt species distribution models. *Divers. Distrib.* **19**, 1366-1379 (2013).
- 35 Rodríguez-Sánchez, F., De Frenne, P. & Hampe, A. Uncertainty in thermal tolerances and climatic debt. *Nature Climate Change* **2**, 636-637, doi:<http://dx.doi.org/10.1038/nclimate1667> (2012).
- 36 Dell, A. I., Pawar, S. & Savage, V. M. Systematic variation in the temperature dependence of physiological and ecological traits. *Proceedings of the National Academy of Sciences* **108**, 10591-10596, doi:10.1073/pnas.1015178108 (2011).
- 37 Brodie, B., Mowbray, F. & Power, D. *OBIS Canada Digital Collections*. <http://www.obis.org/> (Bedford Institute of Oceanography, Dartmouth, NS, Canada, 2013).
- 38 DFO. *OBIS Canada Digital Collections*. <http://www.obis.org/> (Bedford Institute of Oceanography, Dartmouth, NS, Canada, 2016).
- 39 Heessen, H. J., Daan, N. & Ellis, J. R. *Fish Atlas of the Celtic Sea, North Sea, and Baltic Sea: Based on International Research-vessel Surveys*. (Wageningen Academic Publishers, 2015).
- 40 ICES. [https://datras.ices.dk/Data\\_products/Download/Download\\_Data\\_public.aspx](https://datras.ices.dk/Data_products/Download/Download_Data_public.aspx) (ICES, Copenhagen, Denmark, 2015).
- 41 Reid, P. C., Colebrook, J. M., Matthews, J. B. L., Aiken, J. & Team, C. P. R. The Continuous Plankton Recorder: concepts and history, from plankton indicator to undulating recorders. *Progress in Oceanography* **58**, 117 (2003).
- 42 Hirahara, S., Ishii, M. & Fukuda, Y. Centennial-Scale Sea Surface Temperature Analysis and Its Uncertainty. *J. Clim.* **27**, 57-75, doi:10.1175/jcli-d-12-00837.1 (2014).
- 43 Huang, B. *et al.* Extended reconstructed sea surface temperature, version 5 (ERSSTv5): upgrades, validations, and intercomparisons. *J. Clim.* **30**, 8179-8205 (2017).
- 44 Burnham, K. P. & Anderson, D. R. *Model Selection and Multimodel Inference: A Practical Information Theoretic Approach*. 2nd edn, (Springer Verlag, 2002).

**Supplementary Information** is linked to the online version of the paper at [www.nature.com/nature](http://www.nature.com/nature).

## Acknowledgements

M.T.B., B.P., J.G.M. were supported by NERC grant NE/J024082/1; J.G.M. by the "Tenure-Track System Promotion Program" of the Japanese Ministry of Education, Culture, Sports, Science and Technology; D.S.S., G.J.E and R.D.S-S by the Australian Research Council grants DP170101722, LP150100761 and DP170104240, respectively; M.L.P. by National Science Foundation grants OCE-1426891 and DEB-1616821, an Alfred P. Sloan Research Fellowship,

and the NOAA Coastal and Ocean Climate Applications program; and A.E.B. by the Canada Research Chairs Program. Data sources used here are listed in Supplementary Materials.

## **Author contributions**

M.T.B., A.E.B., M.L.P., R.S.-S. and E.S.P. conceived the research. M.T.B. and B.P. analysed the data. M.T.B., A.E.B, B.P, J.G.M. wrote the first draft. All authors contributed equally to discussion of ideas and analyses, and commented on the manuscript.

## **Author information**

The authors declare no competing financial interests. Correspondence and requests for materials should be addressed to M.T.B. (mtb@sams.ac.uk).

## **Affiliations**

<sup>1\*</sup>Scottish Association for Marine Science, Scottish Marine Institute, Dunbeg, Oban, Argyll, PA37 1QA. <sup>2</sup>Ocean and Earth Sciences, National Oceanography Centre Southampton, University of Southampton Waterfront Campus, Southampton SO14 3ZH, UK. <sup>3</sup>Department of Ocean Sciences, Memorial University of Newfoundland, St. John's A1C 5S7, Canada. <sup>4</sup>School of Environment, University of Auckland, Auckland, New Zealand 1142. <sup>5</sup>Sir Alister Hardy Foundation for Ocean Science, The Laboratory, Citadel Hill, Plymouth PL1 2PB, UK. <sup>6</sup>Marine Institute, Plymouth University, Plymouth, PL4 8AA, UK <sup>7</sup>Institute for Marine and Antarctic Studies, University of Tasmania, Hobart, Tasmania, 7001 Australia. <sup>8</sup>Bren School of Environmental Science & Management, University of California Santa Barbara, CA 93106-5131, USA. <sup>9</sup>National Center for Ecological Analysis & Synthesis, University of California, Santa Barbara, CA 93101, <sup>11</sup>School of Ocean Sciences Bangor University, Menai Bridge, Anglesey, LL59 5AB, UK. <sup>12</sup>Department of Ecology, Evolution, and Natural Resources, Rutgers

302 University, 14 College Farm Rd., New Brunswick, NJ 08901, USA. <sup>13</sup>Arctic Research Center,  
303 Hokkaido University, N21W11 Sapporo, Hokkaido 001-0021, Japan. <sup>14</sup>Graduate School of  
304 Environmental Science, Hokkaido University, N10W5 Sapporo, Hokkaido 060-0810, Japan,  
305 <sup>15</sup>School of Science and Engineering, University of the Sunshine Coast, Maroochydore,  
306 Queensland 4558, Australia. <sup>16</sup>Centre for African Conservation Ecology, Department of  
307 Zoology, Nelson Mandela University, Port Elizabeth, South Africa. <sup>17</sup>Alfred Wegener Institute,  
308 Helmholtz Centre for Polar and Marine Research, Division Biosciences/Integrative  
309 Ecophysiology, Am Handelshafen 12, 27570 Bremerhaven, Germany. <sup>18</sup>Global Change Institute,  
310 The University of Queensland, St Lucia, Queensland, Australia.  
311 \*e-mail: mtb@sams.ac.uk.

312

## Figures

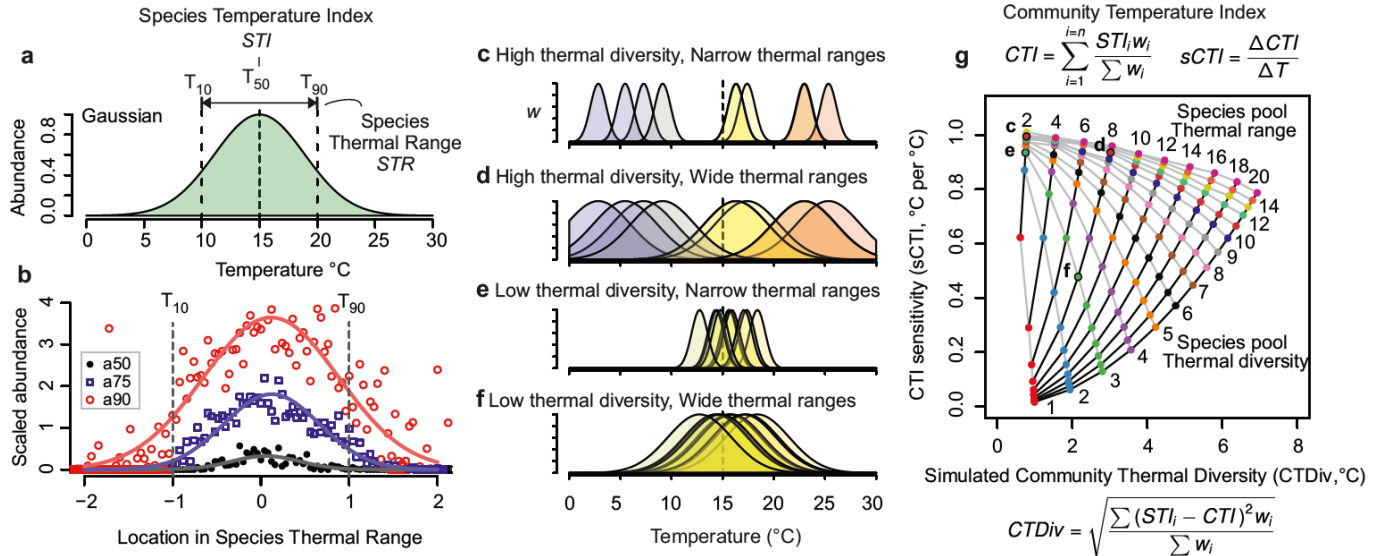


**Fig. 1 | Simulated communities to illustrate the effects of thermal diversity and thermal range width on the sensitivity of Community Temperature Index (CTI) to temperature change.** **a**, a Gaussian abundance-temperature distribution for Species Temperature Index (STI) = 15 and Species Thermal Range (STR) = 10. **b**, quantiles (a50 = 50th percentile etc.) of abundance across thermal ranges for US trawl survey species. **c-f**, Thermal characteristics in simulated pools of species varying in thermal diversity and thermal range, showing subsets forming communities at 15°C mean annual sea temperature. **g**, Sensitivity in simulated communities (symbols) of Community Temperature Index (sCTI, the ratio of CTI change to temperature change) to changing Community Thermal Diversity (CTDiv). Thermal diversity in the species pool (standard deviation of STIs) and the species thermal range were changed for each simulated community of 1000 species, with average sCTIs shown for 1000 repeat runs. Grey lines and similar coloured symbols link simulated communities with the same thermal diversity, black lines linking communities with similar thermal ranges. Letters in **g** indicate the sensitivity of CTI associated with thermal diversity and thermal ranges in the example communities shown in **c-f**.

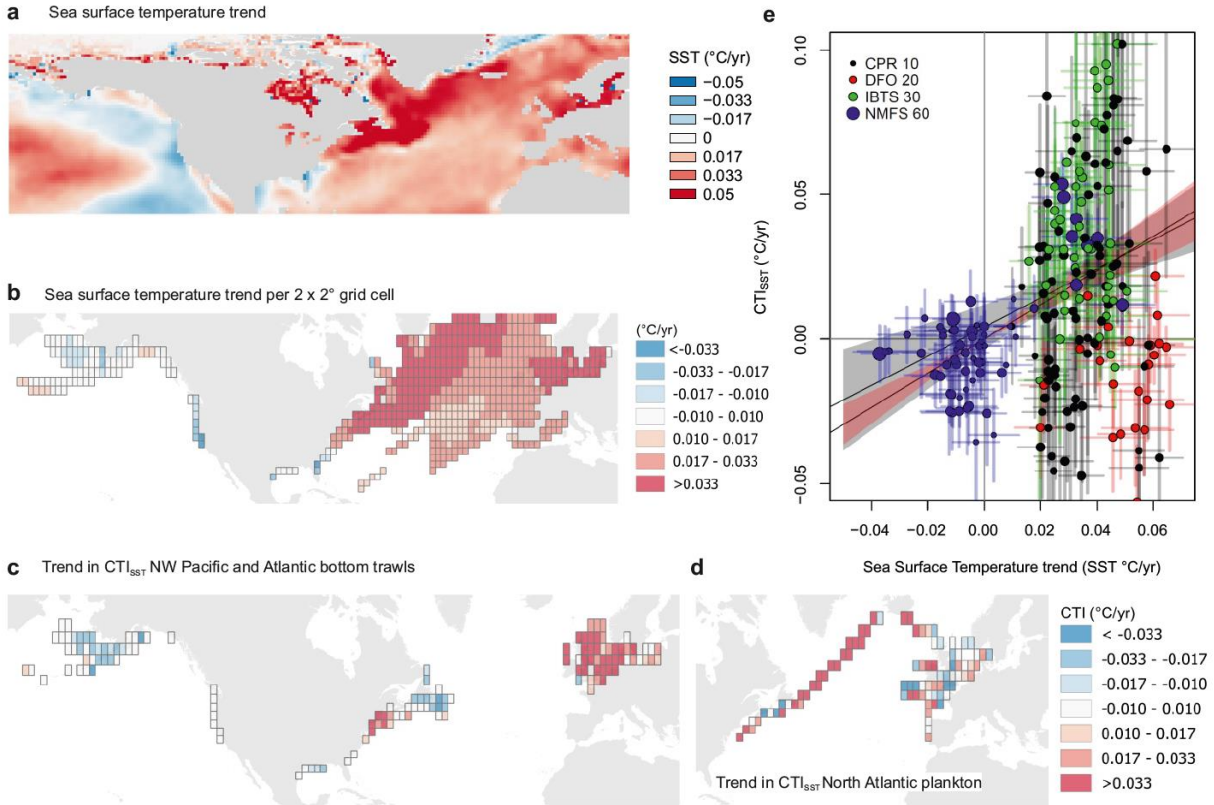


**Fig. 2 | Trends in temperature and composition of demersal and plankton communities shown by Community Temperature Index (CTI<sub>SST</sub>) values from 1985 to 2014.** **a**, Trend in sea surface temperature (SST) from the Hadley Centre Sea Ice and Sea Surface Temperature data set (HadISST v1) where blue is colder and red warmer. **b**, as **(a)** aggregated into the 2° × 2° latitude-longitude grid cells surveyed for plankton and demersal fish. **c**, Trends in CTI<sub>SST</sub> for bottom trawls, and **d**, for Continuous Plankton Recorder hauls. **e**, CTI<sub>SST</sub> trends compared with SST trends. CTI trends are shown as bootstrap averages and standard deviations of computed regression slopes over time (n=500 using random selection of species with replacement). SST trends are shown as regression slopes ± standard errors. Symbol sizes are scaled by the number of years sampled, while colours denote the survey programme (black, CPR, Continuous Plankton Recorder; red, DFO, Department of Fisheries and Oceans, Canada; green, IBTS, International Bottom Trawl Survey; blue, NMFS, US National Marine Fisheries Service). The dependence of CTI<sub>SST</sub> trend on SST trends per gridcell is shown by two regression slopes ± 95% confidence intervals: with an intercept term (solid line with grey shading, Model A, R<sup>2</sup>=0.08) and without (line with red shading, Model B, R<sup>2</sup>=0.23, Supplementary Table 4).

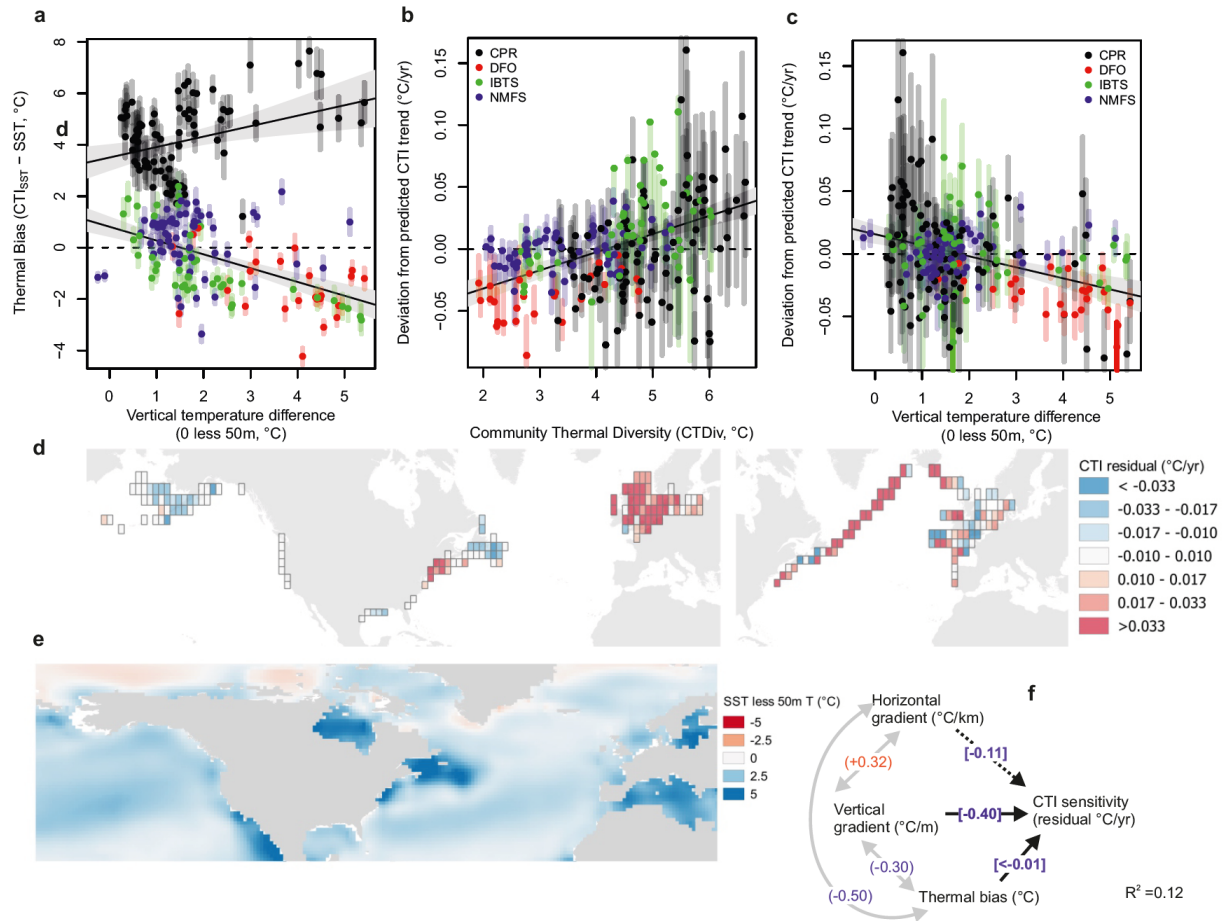


**Fig. 3 | Trends in Community Temperature Index (CTI<sub>SST</sub>) for Northern Hemisphere demersal and plankton communities from 1985 to 2014 influenced by near-surface vertical and horizontal temperature gradients. a**, Thermal bias (CTI<sub>SST</sub> - SST) versus vertical temperature gradient (lower regression through demersal species, upper regression through plankton). **b**, Difference between observed CTI trends and those predicted from surface temperature trends (Model B residuals) versus local Community Thermal Diversity. **c**, Residuals from a regression including SST trends combined with community thermal diversity, community thermal range (Model I residuals, mapped in **d**) versus local vertical temperature difference. Error bars in **a-c** show bootstrap standard errors for CTI<sub>SST</sub> trend estimates. **e**, Vertical temperature gradients (0-50m, 1985-2014 from Hadley Centre EN4 dataset). **f**, Relationships among CTI sensitivity, vertical and horizontal temperature gradients and thermal bias shown by correlation (grey arrows, round parentheses) and regression beta coefficients (black arrows, square parentheses) from regression of residuals from **b** (Supplementary Table 4 Model R1).



## Online only Methods

### Simulation of sensitivity of the community temperature index to temperature change.

Expected effects on the response of community thermal indices to temperature change were explored in a simulation model based on species-level functions relating abundance to temperature. Four functional forms were used: (i) Gaussian, with abundance declining symmetrically away from a central optimum, (ii) a trimmed Gaussian, with a central plateau, and (iii) left- and right-skewed functions based on the gamma distribution (Supplementary Fig. 1). Pools of 1000 species were created by randomly selecting species' thermal midpoints (STI) from a Gaussian distribution with a mean of 15°C plus or minus an offset representing thermal bias<sup>17</sup>, the degree to which the community is composed of types from warmer or colder conditions. Variation in thermal affinities in the species pool was manipulated via the standard deviation of STI values in the species pool, (sdSTI, species pool thermal diversity in Fig. 1e). Each species in the pool was assigned a thermal range (STR, species pool thermal range in Fig. 1e), as the difference between the 90th and 10th percentiles of the abundance-temperature function.

The four abundance-temperature functions (Supplementary Fig. 1) simulated different patterns of abundance across species ranges. The Gaussian function represented species that are more abundant, or occur in a greater proportion of samples, at the centre of the distribution range. In this form, the equivalent standard deviation for a given STR (the difference between the 10<sup>th</sup> and 90<sup>th</sup> percentiles of the distribution) was obtained by dividing STR by  $2 \cdot t_{0.1,\infty}$  (the number of multiples of SD percentiles of a Gaussian distribution). Simulated abundance (or incidence) of any species across the range of temperatures considered, here 0°C to 30°C, was obtained from the probability density function of the Gaussian distribution with the species' STI as the mean and SD-equivalent range width as its standard deviation (as in Fig 1a-d). For the

391 trimmed Gaussian function, simulated abundance between mean–SD and mean+SD was set at  
392 the probability density value for the mean-SD and otherwise followed the standard Gaussian  
393 formulation. For the skewed functions based on the gamma distribution, simulated abundance  
394 was produced using the gamma probability density function for varying shape values, and scale  
395 factors obtained by dividing the STR by the difference between the 90th and 10th percentiles of  
396 each gamma distribution for the applicable shape value and a scale factor of 1.

397 Simulated abundance/incidence values were used to calculate Community Temperature  
398 Index values (CTI, abundance-weighted average STI) and Community Thermal diversity  
399 (CTDiv, abundance-weighted standard deviations of STI values) at different temperatures. The  
400 sensitivity of CTI to temperature change (sCTI) was measured by calculating CTI for species at  
401 temperatures 0.1°C below and above 15°C, and dividing the difference in CTI values by 0.2°C to  
402 give the ratio of CTI change to temperature change.

403 We used linear regression analysis to analyse the response of CTI sensitivity (sCTI) to the  
404 distribution of species thermal properties in these simulated communities. For the Gaussian  
405 abundance-temperature function, CTI sensitivity exactly depended on the squared ratio of CTDiv  
406 to STR (Supplementary Table 3, Model Z), with thermal bias having no meaningful effect.  
407 Adding variable Species Thermal Ranges (Supplementary Table 3, Model Z1) reduced the  
408 sensitivity of CTI to temperature at low levels of thermal diversity, but the effect was relatively  
409 small (Supplementary Table 5). With a flattened response of abundance to temperature emulated  
410 by the trimmed Gaussian function, the negative effect of average species thermal range (CTR)  
411 was completely eliminated. Communities composed of narrow- or wide-ranged species for the  
412 same level of thermal diversity had the same CTI sensitivity (Supplementary Fig. 2b). This

suggests that CTI metrics estimated from range information alone would not be sensitive to the average range width of the species involved for this functional form.

For the asymmetrical abundance-temperature functions represented by the gamma and reversed gamma functions (Supplementary Fig. 1), the effects of varying CTDiv, CTR and the shape of the function were similar in both cases (Models Z3 and Z4, Supplementary Fig. 2c, 2e) but the effects of thermal bias depended on the direction of the skew. For the right-skewed gamma distribution, CTI sensitivity to temperature increased with thermal bias, producing a CTI that would change more rapidly with temperature if composed of warmer-water species. The left-skewed reverse gamma abundance-temperature function, with a shape more similar to physiological temperature performance curves, showed the opposite effect, with more sensitivity of CTI to temperature if the community was composed largely of species from colder waters. This behaviour suggests the rapid changes in abundance at temperatures above the optimum produce more rapid shifts in CTI than the more gradual changes in abundance below the optimum (Supplementary Fig. 1d). Notwithstanding such effects of functional form of the abundance-temperature response on the sensitivity of CTI to temperature, the observed patterns of abundance more closely followed the simple Gaussian function (see section: **Average abundance and incidence across species thermal ranges**).

#### **Marine community data sources.**

Five marine community datasets were used (Supplementary Table 1). For analysis of patterns in responses across spatially extensive time-series data, data from three bottom-trawl survey programs and one plankton sampling program were downloaded and prepared such that every taxon record in each sample (either a single trawl or section of Continuous Plankton Recorder silk) was associated with a latitude, longitude and date. The three bottom-trawl surveys

were organized into different regional sampling programs, and data from each regional program were combined. US National Marine Fisheries Service (NMFS) data were obtained from the Ocean Adapt website and pre-processed using existing R code (Pinsky group, <https://github.com/pinskylab/OceanAdapt> downloaded February 2016). European International Bottom Trawl Survey (IBTS) datasets were downloaded in a common format with details of sizes of species caught and of each trawl, of which only the abundance, date and location were used. Canadian Department of Fisheries and Oceans data came from the Ocean Biogeographical Information System (OBIS) web portal, with similar details of sampling. Continuous Plankton Recorder data were obtained directly from the Continuous Plankton Recorder Survey, including date of hauls, longitude and latitude alongside estimated species abundance.

Each dataset recorded abundance in a different way but, for every dataset including those that lacked abundance data, analyses were possible using species incidence among samples taken in the aggregating location and period. Species incidence (the relative frequency of trawls in which the species occurred, for data aggregated by area and time period) was used as the weighting factor in all calculations of community thermal metrics (CTI, CTDiv, CTR), and was highly correlated with abundance when available (Supplementary Fig. 10).

#### **Ocean temperature data.**

We used five sea-surface-temperature datasets and one layered subsurface dataset for analysis of temperature change in the study region (Supplementary Table 1). Annual sea surface temperatures per 1° latitude-longitude grid cell were averaged over 1985 to 2014 for each dataset to represent long-term climate over the period of surveys. Seabed temperatures were derived from the deepest layer in the Hadley Centre EN4 dataset and averaged over the same period. Trends in °C/yr were calculated for 1° cells using annual means from 1985 to 2014 (Fig. 2e,

Supplementary Fig. 13). Vertical gradients in temperature (Fig. 3d) were calculated using the EN4 dataset<sup>25</sup> from layer means (surface: 5.02m, “50m”: 45.4m, “100m”: 98.3m, “200m”: 207.4m) based on annual means from 1985 to 2014 .

#### **Derivation of Species Temperature Indices (STIs) and fitted Maxent models.**

Global predicted distribution maps were produced using presence-only Maxent models for each species in fish and plankton datasets occurring in ten or more 1° cells, and using default parameters for a random seed, convergence threshold, maximum number of iterations, maximum background points and the regularization parameter<sup>3</sup> (Maxent version 3.3.3k). Observations of species presence from OBIS were gridded such that 1° grid cells with observations were set as present. Only 2% of species were found in <10 1°latitude/longitude gridcells, with most species found in 10 to 100 gridcells (10-32, 36%; 32-100, 37%; >100, 24%). These observations were then modelled as a function of the following environmental predictors: (1) average annual temperatures from the HadISST v1.1; (2) the logarithm of distance to the nearest coastline; (3) ocean depth from the GEBCO marine atlas; and (4) FAO major fishing areas (<http://www.fao.org/fishery/area/search/en>). Frequency of all records in OBIS in 1° grid cells was used as the bias correction file. Although we did not additionally spatially thin the input records as has been suggested<sup>34</sup>, the reduction of records to presence in 1° cells and inclusion of the bias file were attempts to reduce spatial bias due to uneven sampling effort. Global maps of predicted presence were produced using a threshold probability of 0.4, restricting the range of possible areas to those of high suitability<sup>4</sup>.

Resulting Maxent-predicted distribution maps were used to extract sea temperature values from long-term climatology average 1985-2014 from HadISST (henceforth CTIhadsst1), EN4 surface (CTIen4sst) and EN4 seabed (CTIen4sbt). Quantiles (0, 0.1, 0.25, 0.5, 0.75, 0.9 and 1.0,

area-weighted by the cosine of the latitude) of these map-extracted temperatures were used to define the thermal niche of the species. The 50<sup>th</sup> percentile (median) of temperatures in occupied areas was used as the Species Temperature Index (STI, derived separately for HadISST and EN4 SST and seabed). The difference between 10<sup>th</sup> and 90<sup>th</sup> percentile temperatures ( $T_{90} - T_{10}$ , Fig. 1a) defined the Species Thermal Range (STR). A Species Temperature Index derived as the average of  $T_{90}$  and  $T_{10}$  values obtained from species presence in 1° grid cells was also used to (i.e. not Maxent modelled STIhadsst2)

Patterns in ocean temperature were used twice in the analysis: (i) as long-term mean values matched to modelled species distributions to derive STIs and STRs, and (ii) as local trends over the 30-year study period to compare with local trends in CTI values. Despite the use of information on sea temperature more than once, information flows in the derivation of species thermal affinities and analysis of spatial patterns were separate from those in the analysis of temporal patterns in community thermal composition related to temperature trends (Supplementary Fig. 4). These separate pathways allowed us to avoid circularity in reasoning.

#### **Average incidence (relative frequency of occurrence) across species thermal ranges.**

The form of the relationships of species incidence with range location was determined by first matching species' incidence to local temperatures in 2° grid cells, and then locating those temperatures relative to the thermal limits of the distribution of each species (Fig. 1b, Supplementary Fig. 3). Average incidence values were calculated for every species in 2° latitude-longitude grid cells as the frequency of samples in which the species occurred, expressed as a proportion of the total number of samples across the whole period of each survey. Range

location was derived from the average temperature in the cell relative to range limits (Fig. 1b,  $T_{10}$  and  $T_{90}$ , equation in Supplementary Table 2).. Incidence values per  $2^\circ$  cell were rescaled for every species to give values relative to the average incidence within the STR, so reducing the effect of prevalent species on the resulting pattern. Percentiles (50%, 75%, 90%) of scaled-incidence values were then calculated in range-location unit classes of  $1/25$  from -2 to 2 (Fig. 1b, Supplementary Fig. 3). To check how well incidence reflected species abundance, calculations were repeated for abundance measures where available (average weight per trawl for NMFS data and number per haul for CPR and IBTS data) by summing numbers or biomass and dividing this sum by the total number of samples in each  $2^\circ$  latitude-longitude grid cell (Supplementary Fig. 3). Abundance changes across thermal ranges were calculated in the same way as incidence changes.

**Community Temperature Index (CTI), Thermal Diversity (CTDiv), average Species Thermal Range (CTR) and Thermal Bias in surveys.**

CTI values were calculated as incidence-weighted average STIs using data aggregated in  $2^\circ \times 2^\circ$  grid  $1^\circ$  grid cells to produce maps (Supplementary Figures 4 and 9), and temporal trends (Fig. 2). Community thermal diversity, CTDiv, the spread of STI values around each CTI measure, was similarly calculated as the incidence-weighted standard deviation of the STIs for species present in the grid cell or grid cell/ year combination. Community thermal range (CTR) was the incidence-weighted average of species' STR values. Incidence (relative frequency of species in samples per aggregation unit) was used as the weighting factor because abundance was expressed differently in each dataset (Supplementary Table 1): as total numbers per trawl sample (IBTS data), biomass per haul (NMFS data), and as scores per silk (CPR data). However, incidence was strongly related to abundance in each set for which abundance data were available

(Supplementary Fig. 8). Thermal bias was calculated as the CTI minus local sea temperature (using whichever temperature dataset was used to derive corresponding STIs), giving positive values where more species were from warmer areas and negative values where the species were from cooler places.

Uncertainty in CTI estimation is often poorly estimated<sup>35</sup> so, in addition to the four alternative methods of derivation of STIs, we used bootstrap resampling of species to generate standard errors and confidence intervals for means and trends in CTI and for the outcomes of more complex regression analyses. Bootstrap sets of species were randomly selected with replacement from those in each survey scheme (141 CPR, 285 IBTS, 585 NMFS, and 285 DFO species). The frequency of each species in the bootstrap set was used as a multiplier on species incidence as the weighting factor ( $w_i$  in Supplementary Table 2) to give bootstrap estimates of each of the community thermal metrics. Each metric (annual mean, anomaly, trend) and regression model was computed for 500 repeated bootstrap species selections, and summarised to give bootstrap averages, standard errors and 95% confidence intervals.

For time-series analysis, the annual CTI values averaged per  $2^\circ \times 2^\circ$  grid cell were expressed as an anomaly from the 1985-2014 average CTI for that cell. US NMFS data had several regional series that occurred together in the same grid cell, notably in the Northeast and Southeast US spring and fall series. In this case, anomalies were calculated for each series separately then averaged to give final CTI values for that cell. Trends in CTI for each  $2^\circ \times 2^\circ$  cell were calculated using all years for which CTI values were available, and matching trends for SST values were calculated for the same set of years.



## **Uncertainty in annual CTI anomalies and temporal trends: data filtering**

The magnitude of CTI anomalies from long-term means in  $2^\circ \times 2^\circ$  grid cells shows the effect of sampling effort on the uncertainty in these estimates (Supplementary Fig. 11a, b). As expected, given the standard error of the mean being proportional to the underlying standard deviation multiplied by the square root of the sample size, the magnitude of anomalies declined with the number of species records (STIs) used to compute each CTI value (Supplementary Fig. 11a). CTI anomalies were omitted from trend analysis for bottom-trawl surveys if comprising fewer than 20 species records. Similarly, annual CTI anomalies tended to be larger when composed of fewer bottom trawls or plankton samples. Estimates based on fewer than 10 bottom trawls or plankton hauls per year were also excluded from further analysis (Supplementary Fig. 11b).

Standard errors associated with trends in CTI over time in each  $2^\circ \times 2^\circ$  grid cell were also related to the number of years sampled and the total species records over the time series in each cell (Supplementary Fig. 11c, d). Trends based on fewer than 10 years of data and less than 1000 species records were omitted from further analysis.

## **Analysis of trends in CTI versus community thermal traits: community thermal diversity (CTDiv), average thermal range width (CTR) and thermal bias, and predictions of sensitivity from simulated communities.**

Relationships between trends in Community Temperature Index (as bootstrap-mean  $CTI_{SST}$ ) and trends in sea temperature (HadISST), as modified by community thermal affinities, were analyzed by fitting least-squares multiple linear regression models (Supplementary Table 4). The relative importance of models was evaluated using Akaike weights. Intercepts were omitted from models because no CTI change would be expected where the temperature trend was zero (unless

there was some delayed shift from an earlier period of warming or cooling). Adding intercepts back into these models (Models A and Ci to Ni) had very little effect on model fits (as shown by  $\Delta AICc$ ) or the parameter value estimates, and did not result in intercepts that were significantly different from zero.

Terms were introduced first as linear effects and then as squared terms, reflecting the results from the simulation model (Model Z). Modifying effects of average community thermal metrics (CTDiv, CTR, Thermal bias) and local vertical and horizontal gradients in average temperature were expressed as interactions with the temporal trend in sea surface temperature to address sensitivity of CTI to temperature. Considering effects only as interaction terms reflected the assumption that change in average thermal affinity would respond to changes in temperature, and that patterns of local average thermal diversity, species range, or thermal bias would modify that change in CTI in response to temperature. The model with the squared ratio of community thermal diversity (CTDiv) to species thermal range (CTR, Model G) links the observational data with the simulation analysis. In simulations using the Gaussian function, regression of log CTI sensitivity on log STR (=CTR in this case, since all species in the simulation had the same STR) and CTDiv gave a perfect fit with coefficients of -2 and 2 respectively, which back transforms from logs to the one-parameter equation involving the squared ratio of CTDiv to CTR (Model Z).

Adding the interactive effect of thermal diversity (CTDiv) to SST trend (dSST) produced a better model (Model D vs B,  $AIC_{CD} - AIC_{CB} = -63.90$ ), while adding thermal range (CTR) alone did not (Model C vs B,  $AIC_{CC} - AIC_{CB} = -2.52$ ). Including both factors, either as linear predictors (E) or squared terms (F), further improved the model (Model E vs B,  $AIC_{CE} - AIC_{CB} = -82.62$ ; Model F vs B,  $AIC_{CF} - AIC_{CB} = -77.03$ ). Thermal diversity was negatively correlated with

inverse thermal range width, resulting in large changes in parameter values when each factor was added to a model containing the other. The squared-ratio model ( $CTDiv^2:CTR^2$ ), Model G, equivalent to the model fitted to simulation data (Z), had similar explanatory power to other models including those terms (E, F). The parameter value for this model (G, 7.63) was close to the 6.54 obtained for simulated communities (Z).

Thermal bias affected CTI sensitivity in the simulations, negatively or positively depending on the direction of skew of the abundance-temperature relationship, and so was introduced as an addition to the squared ratio model. Adding thermal bias slightly improved model fit (Model H vs G,  $AIC_{CH} - AIC_{CG} = -1.18$ ) and increased the sensitivity of CTI by 0.04 for each °C of thermal bias. This positive effect meant that communities comprising warm-water species showed greater change in CTI than those composed of cold-water species for the same change in temperature. The effect was also consistent with the effect of realized right-skewed (gamma) abundance-temperature distribution in the simulations, but not a left-skewed one as implied by typical physiological thermal performance curves<sup>36</sup>.

Both horizontal and vertical gradients in temperature were expected to influence CTI sensitivity. Steep vertical gradients in temperature may have a negative effect on CTI sensitivity because species may be able to shift to cooler temperatures in the same area by moving deeper. Gentle horizontal gradients in temperature, combined with temperature change through time, result in higher velocities of climate and thereby more rapid distribution shifts among species<sup>2,18</sup>. With a greater rate of species turnover in areas of high climate velocity, we expected a negative relationship between CTI sensitivity and the magnitude of the horizontal gradient in temperature. Adding shallow vertical temperature differences (surface less 50m) improved the model with community thermal diversity and thermal range (Model I vs G,  $AIC_{CI} - AIC_{CG} = -33.39$ ), albeit

with no effect of vertical differences from surface to 100m (Model J) or 200m depth (Model K). Adding horizontal temperature gradient (Model L) to the basic model (G) had a smaller effect on model fit ( $AIC_{cL} - AIC_{cG} = -3.15$ ) and did show the expected negative influence of the horizontal gradient. Combining vertical and horizontal gradients in temperature (Model M) did not improve model fit, and the horizontal gradient coefficient did not differ from zero. A regression model that included thermal bias effects as well as horizontal and vertical gradients in temperature (Model N) was the most parsimonious, albeit with the parameter for horizontal gradient not significantly different from zero. Residuals from the squared-ratio model proved to be related most strongly to the effect of vertical temperature gradient (Model R1, Fig. 3b).

Cross validation of was used to examine the predictive skill of Model I (Supplementary Table 4, Supplementary Fig. 12). We used dataset type (bottom trawls or plankton) and latitude and longitude (giving contiguous spatial blocks) to split the data into near similar-sized training and test datasets, with each set alternately used as the training set for the other test set of data. Choices of splits for latitude (50°N) and longitude (40°W) were arbitrary, but adopted to produce adequately sized datasets for fitting. Model I fitted to the plankton subset as training data (Model Icpr) and bottom-trawl subsets (Model Idem) produced similar parameter estimates (significant  $P < 0.05$ ), with CTI trends for bottom trawls explained markedly better. Splitting into plankton and demersal species gave the worst fits to the other as test data (CV rsme 0.0284), the plankton training set predicting larger CTI trends than the bottom-trawl training set. Splitting by latitude and longitude gave similar root mean squared errors to the plankton / bottom-trawl split (Supplementary Table 4), but produced non-significant parameter estimates for the vertical temperature gradient term for data west of 40°W. Model residuals for Model I showed some

spatial structure (Supplementary Fig. 12a), with evidence for spatial autocorrelation in the CTI trends and in the predictor variables (Supplementary Fig. 12b-c).

Of all predictors tested beyond the effects of thermal diversity and thermal range, the vertical temperature gradient effect had the largest influence on CTI sensitivity, (Fig. 3f). The apparent positive effect of thermal bias was due to the negative association with vertical gradient for demersal species (Fig. 3a), and the small negative effect of horizontal gradient was due to the weak positive association of vertical and horizontal gradients of temperature, particularly in the northwest Atlantic.

#### **Evaluation of explanatory power of alternate sea temperature datasets in explaining spatial variation in trends in CTI anomalies**

We fitted a subset of regression models in Supplementary Table 4 to every combination of four variants of CTI and temperature trends from nine dataset layers: five surface layers (EN4SST, COBESST, ERSST, HadISST and OISST, Supplementary Fig. 13) and four subsurface layers (EN4SBT, EN4 50m depth, EN4 100m depth and EN4 200m depth). Models were fitted for every bootstrap selection of species ( $n=500$ ), with model fits and 95% bootstrap confidence intervals shown in Supplementary Fig. 14. The most variation in CTI was explained for  $CTI_{SST}$  from STIs obtained by matching modelled species distributions to surface temperature (aCTI<sub>en4sst</sub> and aCTI<sub>hadsst1</sub>), with the poorest performance of models fitted to  $CTI_{SST}$  from STIs obtained by matching 1° mapped observations of species presence in gridcells (from OBIS data summed for the period 1960 to 2009) to surface temperatures (aCTI<sub>hadsst2</sub>). Trends in seabed temperatures did least well in terms of adjusted  $R^2$  at predicting  $CTI_{SBT}$  or  $CTI_{SST}$ . Models that included terms for the squared ratio of thermal diversity to range width fitted better when in combination with magnitude of vertical gradient and/or horizontal gradient.

662

663 **Data availability**

664 The data that support the findings of this study are available at the publicly accessible  
665 repositories listed in Supplementary Table 1.

666

667 **Data Availability Statement**

668 The Community Temperature Index (CTI) values and species thermal affinity data that support  
669 the findings of this study are available in figshare with the identifiers  
670 <https://doi.org/10.6084/m9.figshare.9699068> for annual values and 30 year means  
671 (Supplementary Fig. 7), <https://doi.org/10.6084/m9.figshare.9699107> for trends in  $2^{\circ} \times 2^{\circ}$  grid  
672 cells (Figs 2, 3, Supplementary Fig. 5), and <https://doi.org/10.6084/m9.figshare.6855203.v1> for  
673 species thermal affinities. Source data for the analyses presented are available at links given in  
674 the supplementary information files. Source code for the simulation of CTI response to  
675 temperature change is available at <https://github.com/michaeltburrows/ctisimulation> (Fig. 1).

**Supplementary Table 1 | Datasets used in analyses of spatial and temporal trends in community average thermal traits.**

**Ecological community datasets.**

<b>Name</b>	<b>Area</b>	<b>Short</b>	<b>Source / Access date</b>	<b>Reference</b>	<b>Abundance</b>
US National Marine Fisheries Service	North Atlantic, Gulf of Mexico, North Pacific	NMFS	<a href="http://oceanadapt.rutgers.edu/">http://oceanadapt.rutgers.edu/</a> (11/2/2016)	Pinsky et al 2013 <sup>2</sup>	Wet weight
Department of Fisheries and Oceans Canada	Canada Maritimes, Newfoundland and Labrador	DFO	<a href="http://www.iobis.org/">http://www.iobis.org/</a> i. DFO Newfoundland and Labrador Region Ecosystem Trawl Surveys ii. DFO Maritimes Research Vessel Trawl Surveys Fish Observations (6/5/2016)	Use: Pinsky et al 2013 <sup>2</sup> Data citation: i. Brodie et al 2013 <sup>37</sup> ii. DFO <sup>38</sup>	Presence only
International Bottom Trawl Surveys	NW European shelf	IBTS	ICES DATRAS ( <a href="https://datras.ices.dk/Data_products/Download/Download_Data_public.aspx">https://datras.ices.dk/Data_products/Download/Download_Data_public.aspx</a> ) (30/10/2015)	Use: Heessen et al 2015 <sup>39</sup> Data citation: ICES <sup>40</sup>	Number per haul
Continuous Plankton Recorder Survey	North Atlantic	CPR	CPR Survey (URL by application: <a href="https://www.cprsurvey.org/data/data-request-form/">https://www.cprsurvey.org/data/data-request-form/</a> ) (16/10/2015)	Use: Reid et al 2003 <sup>41</sup>	Categories, abundance per area of silk

**Supplementary Table 1 (continued)****Sea temperature datasets**

Dataset	Description	Portal	Accessed
HadISST v1.1 <sup>24</sup>	Hadley Centre Sea Ice and Sea Surface Temperature data set	<a href="https://www.metoffice.gov.uk/hadobs/hadisst/data/download.html">https://www.metoffice.gov.uk/hadobs/hadisst/data/download.html</a>	31/07/2017
COBESSTv5 <sup>42</sup>	A centennial sea surface temperature (SST) analysis	<a href="ftp://ftp.cdc.noaa.gov/Datasets/COBE2/sst.mon.mean.nc">ftp://ftp.cdc.noaa.gov/Datasets/COBE2/sst.mon.mean.nc</a>	18/05/2018
ERSSTv5 <sup>43</sup>	Extended Reconstructed Sea Surface Temperature (ERSST) v5. 2° monthly average temperatures. Dataset DOI: 10.7289/V5T72FNM	<a href="ftp.ncdc.noaa.gov/pub/data/cmb/ersst/v5/netcdf">ftp.ncdc.noaa.gov/pub/data/cmb/ersst/v5/netcdf</a>	18/05/2018
OISST	NOAA Optimum Interpolation (OI) Sea Surface Temperature (SST) V2. 1° monthly average temperatures .	<a href="https://www.esrl.noaa.gov/psd/data/gridded/data.noaa.oisst.v2.html">https://www.esrl.noaa.gov/psd/data/gridded/data.noaa.oisst.v2.html</a>	18/05/2018
HadEN4 <sup>25</sup>	EN4.2.0. Objective analyses of quality controlled subsurface ocean temperature profiles. 1° monthly average temperatures at 43 depth layers, aggregated into yearly averages	<a href="https://www.metoffice.gov.uk/hadobs/en4/download.html">https://www.metoffice.gov.uk/hadobs/en4/download.html</a>	02/08/2017



**Supplementary Table 2 | Definitions of species' and community thermal trait metrics.**

Abbr	Metric	Definition	Note
STI	Species Thermal Index	$STI = T_{50}$ the temperature at the 50 <sup>th</sup> percentile of temperatures experienced throughout the species range	Ranges predicted using Maxent models fitted to occurrence data in OBIS.
STR	Species Thermal Range	$STR = T_{90} - T_{10}$ the difference between 10 <sup>th</sup> percentile and 90 <sup>th</sup> percentile temperatures of the species range	Species-level measure of the temperature range across their distribution.
CTI	Community Temperature Index	$CTI = \frac{\sum_{i=1}^N STI_i w_i}{\sum w_i}$ where $w_i$ is the weight for species $i$ , and $N$ is the number of species in the community (in single surveys or aggregated across areas and years)	Community-level measure of average species thermal affinity. Weighted average of Species Thermal Indices calculated for a community. Incidence (relative frequency of occurrence in grouped samples) was used as the weight in analyses.
CTR	Community Thermal Range	$CTR = \frac{\sum_{i=1}^N STR_i w_i}{\sum w_i}$	Community-level measure of average species thermal range width, here weighted by incidence.
CTDiv	Community Thermal diversity	$CTDiv = \sqrt{\frac{\sum (STI_i - CTI)^2 w_i}{\sum w_i}}$	Community-level measure of cross-species variation in thermal affinity. Weighted standard deviation of STI values across community members.
	Thermal bias	Thermal bias = CTI – SST	The difference between CTI and local sea surface temperature.
sCTI	CTI Sensitivity	$sCTI = \frac{\Delta CTI}{\Delta SST}$	Change in CTI per change in SST.
	Range location	$RL = 2 \frac{T_{local} - T_{10}}{STR} - 1$	Scaled range location for abundance-temperature relationships among species

**Supplementary Table 3.** Summary of effects of types of abundance-temperature relationships on sensitivity of CTI to temperature change (sCTI) based on linear regression. Values shown are regression coefficients ( $\pm$  standard errors). A full list of parameter estimates is given in Supplementary Table 5.

Model	Functional type	Plot	log10 (CTDIV)	log10 (STR)	Thermal bias	sdSTR / Shape
(parameter ranges)			(1 to 15)	(2 to 20 by 2)	(-5 to 5 by 1)	
Z	Gaussian	Fig. 1f	2.00 (1 to 15)	-2.00 (4 to 12 by 2)	0.00 (-5 to 5 by 1)	( <b>sdSTR</b> : 0.001, 1 to 4)
Z1	Gaussian plus variable STR	Supplementary Fig. 2a	2.00	-2.00	Sensitivity declines as thermal bias increases	<b>sdSTR</b> : Negative effect. CTI sensitivity ( <b>sCTI</b> ) declines as variation in STR increases. Interacts to reduce negative STR effect as variability in STR increases, but has little influence on the effect of thermal diversity.
Z2	Trimmed Gaussian	Supplementary Fig. 2b	1.93 (1 to 15)	0, Effect of thermal range width is removed (4 to 12 by 2)	Negligible (-5 to 5 by 1)	( <b>Shape</b> : 1 to 4)
Z3	Gamma (right-skewed)	Supplementary Fig. 2c, 2d	0.97 (0.05)	-1.03 (0.05)	Positive, sensitivity increases with thermal bias	<b>Shape</b> : >1 increases sensitivity. Increases positive effects of thermal diversity and negative effects of thermal range width towards the Gaussian values (+2 and -2)
Z4	Reversed gamma (left-skewed)	Supplementary Fig. 2e, 2f	0.92 (0.05) (shape 1)	-1.01 (0.05)	Negative, sensitivity declines with thermal bias	<b>Shape</b> : >1 increases sensitivity. Increases positive effects of thermal diversity and negative effects of thermal range width towards the Gaussian values (+2 and -2)

1 **Supplementary Table 4 | Parameter estimates ( $\pm$  standard error) from regression models fitted to bootstrap mean HadISST-derived CTI<sub>SST</sub>**  
2 **trends among  $2^\circ \times 2^\circ$  grid cells** (n=215), using CPR, NMFS, IBTS and DFO data combined. Definitions of terms are given in Supplementary Table 2.  
3 Model Z gives the dependence of CTI sensitivity to temperature change on the squared ratio of community thermal diversity (CTDiv) and range width  
4 (CTR) in the simulation model (Fig. 1g). Models B to G include thermal diversity (CTDiv, CTDiv<sup>2</sup>) and inverse community thermal range (invCTR,  
5 invCTR<sup>2</sup>) as interaction terms with temporal trend in sea surface temperature (dSST). Models H to K add thermal bias (thermbias) to these models, while  
6 models I to M add the effect of local horizontal (mnsgr) and vertical gradients in temperature (slessdeep, differences between surface and deeper layers:  
7 50m, 100m, and 200m) as covariates from EN4 analysis products. Model weights<sup>44</sup> give the relative likelihoods of each model based on  $\Delta$ AIC relative to  
8 Model N. Cross validation of Model I used training data subsets split by plankton and demersal species (Icpr, Idem), north and south of 50°N (INorth,  
9 ISouth), and east and west of 40°W (IWest, I East). Cross-validation root mean squared error (CV rmse) measured model skill.

M#	Description	$\Delta$ AICc	Model weight, w	R <sup>2</sup>	Adj R <sup>2</sup>	Intercept	dSST	dSST x CTDiv(^2)	dSST x CTDiv <sup>2</sup> x invCTR <sup>2</sup>	dSST x invCTR(^2)	dSST x mnsgr	dSST x slessdeep	dSST x thermbias
Z	<b>Simulations</b>								6.54				
A	SST trends effect	85.42	0.00	0.08	0.08	0.004 $\pm$ 0.004§	0.47 $\pm$ 0.11						
B	SST trends effect, no intercept	84.57	0.00	0.23	0.22		0.56 $\pm$ 0.07						
C	Thermal Range width	82.06	0.00	0.24	0.24		1.19 $\pm$ 0.30			-9.37 $\pm$ 4.37			
D	Thermal diversity	20.68	0.00	0.43	0.43		-1.33 $\pm$ 0.22	0.43 $\pm$ 0.05					
E	Thermal range plus thermal diversity	1.95	0.11	0.48	0.48		-3.70 $\pm$ 0.55	0.62 $\pm$ 0.06		22.45 $\pm$ 4.83			
F	as squared terms	7.54	0.01	0.47	0.46		-1.56 $\pm$ 0.29	(0.07 $\pm$ 0.01)		(146.62 $\pm$ 34.24)			
G	combined	33.69	0.00	0.39	0.39				7.63 $\pm$ 0.65				
H	Thermal bias effect	32.51	0.00	0.40	0.39				7.33 $\pm$ 0.67				0.04 $\pm$ 0.02§
I	Vertical gradient effects: using 50m	0.30	0.32	0.48	0.48				11.14 $\pm$ 0.83			-0.16 $\pm$ 0.03	
J	100m	164.94	0.00	0.44	0.43				11.99 $\pm$ 1.07			-0.16 $\pm$ 0.03	
K	200m	347.31	0.00	0.29	0.28				7.89 $\pm$ 1.36			-0.03 $\pm$ 0.05§	
L	Horizontal gradient effect	30.54	0.00	0.40	0.40				8.84 $\pm$ 0.83		-18.55 $\pm$ 8.10		
M	Vertical plus horizontal gradient effects	0.52	0.27	0.49	0.48				10.86 $\pm$ 0.85		12.66 $\pm$ 9.24§	-0.19 $\pm$ 0.03	
N	Thermal bias, combined with vertical gradient effects	0.00	0.30	0.49	0.48				10.53 $\pm$ 0.87		13.39 $\pm$ 9.22§	-0.18 $\pm$ 0.03	0.03 $\pm$ 0.02§
Cross-validation of Model I		Subset rmse	CV rsme										
Icpr	Model I for CPR data (n=84)	0.0362	0.0284	0.51	0.49				21.80 $\pm$ 2.49			-0.42 $\pm$ 0.07	
Idem	Model I for bottom trawl data (n=131)	0.0221		0.61	0.60				9.25 $\pm$ 0.68			-0.12 $\pm$ 0.02	
INorth	Model I for >50°N (n=94)	0.0306	0.0302	0.60	0.60				11.62 $\pm$ 1.02			-0.11 $\pm$ 0.05	
ISouth	Model I for <=50°N (n=121)	0.0299		0.23	0.21				8.35 $\pm$ 1.60			-0.13 $\pm$ 0.04	
IWest	Model I for <40°W (n=108)	0.0234	0.0321	0.48	0.47				13.55 $\pm$ 1.39			-0.21 $\pm$ 0.03	
IEast	Model I for >=40°W (n=107)	0.0362		0.49	0.49				10.08 $\pm$ 1.18			-0.10 $\pm$ 0.06§	

10

11 Values in parentheses give the parameter estimate for the squared value of the community thermal metric (dSST x CTDiv<sup>2</sup>, dSST x invCTR<sup>2</sup>). § denotes  
12 coefficients not significantly different from zero at P<0.05.

13  
14  
15  
  
  
16  
17  
18  
19  
20

**Supplementary Table 4 (continued) | Regression models fitted to CTI trends.** Models shown here (Ci to Ni) are the same as C to N above with added intercept terms to allow a non-zero change in CTI for zero change in temperature.

M#	Description	ΔAICc	Model weight, w	R <sup>2</sup>	Adj R <sup>2</sup>	Intercept	dSST	dSST x CTDiv(^2)	dSST x invCTR <sup>2</sup>	dSST x invCTR(^2)	dSST x mnsg	dSST x slessdeep	dSST x thermbias
Ci	Thermal Range width	83.90	0.00	0.10	0.09	0.002 ± 0.004§	1.11 ± 0.35			-8.74 ± 4.55§			
Di	Thermal diversity	22.68	0.00	0.32	0.31	-0.001 ± 0.003§	-1.32 ± 0.23	0.43 ± 0.05					
Ei	Thermal range plus thermal diversity	3.75	0.11	0.38	0.37	0.002 ± 0.003§	-3.78 ± 0.57	0.62 ± 0.06		23.04 ± 4.94			
Fi	as squared terms	8.98	0.01	0.37	0.36	0.003 ± 0.003§	-1.66 ± 0.31	(0.07 ± 0.01)		(153.66 ± 35.26)			
Gi	combined	35.43	0.00	0.27	0.27	-0.002 ± 0.003§			7.99 ± 0.90				
Hi	Thermal bias effect	33.41	0.00	0.28	0.28	-0.003 ± 0.003§			7.97 ± 0.89				0.04 ± 0.02
Ii	Vertical gradient effects: using 50m	0.68	0.32	0.39	0.38	0.004 ± 0.003§			10.59 ± 0.92			-0.17 ± 0.03	
Ji	100m	165.17	0.00	0.33	0.32	0.005 ± 0.003§			11.19 ± 1.22			-0.16 ± 0.03	
Ki	200m	348.93	0.00	0.13	0.12	0.003 ± 0.004§			7.08 ± 1.79			-0.03 ± 0.05§	
Li	Horizontal gradient effect	32.66	0.00	0.29	0.28	0.000 ± 0.003§			8.86 ± 0.97		-18.47 ± 8.36		
Mi	Vertical plus horizontal gradient effects	1.20	0.27	0.39	0.38	0.004 ± 0.003§			10.38 ± 0.94		11.75 ± 9.26§	-0.19 ± 0.03	
Ni	Thermal bias, combined with vertical gradient effects	1.57	0.30	0.39	0.38	0.002 ± 0.003§			10.27 ± 0.94		12.67 ± 9.27§	-0.19 ± 0.03	0.02 ± 0.02§
R1	Residual from Model G vs vertical and horizontal gradients and thermal bias			0.14	0.12	0.020 ± 0.006					0.759 ± 0.468§	-0.010 ± 0.002	-0.0003 ± 0.0008§

Values in parentheses give the parameter estimate for the squared value of the community thermal metric (dSST x CTDiv<sup>2</sup>, dSST x invCTR<sup>2</sup>). § denotes coefficients not significantly different from zero at P<0.05.

**Supplementary Table 5.** Parameter estimates from linear regression analysis of CTI sensitivity (log10 transformed) in simulated communities using different types of abundance-temperature functions (see Supplementary Fig. 1). Results are summarised in Supplementary Table 3, including the ranges of input parameters. Abbreviations: CTDiv, Community Thermal Diversity; CTR, Community Thermal Range; sdSTR, standard deviation in Species Thermal Range; thermbias, Thermal Bias; shape, gamma shape parameter. Interactions are denoted by x between two terms.

Model Z1, Adjusted  $R^2 = 0.9243$ . Gaussian function with variable STR

Term	Estimate	Std. Error	t value
Intercept	0.786	0.018	44.24
log10(CTDiv)	1.998	0.022	88.90
log10(CTR)	-1.997	0.025	-80.05
sdSTR = 1	-0.058	0.024	-2.39
sdSTR = 2	-0.167	0.024	-6.87
sdSTR = 3	-0.222	0.025	-8.74
sdSTR = 4	-0.161	0.027	-5.88
thermbias = -4	0.013	0.006	2.02
thermbias = -3	0.025	0.006	4.02
thermbias = -2	0.038	0.006	6.06
thermbias = -1	0.052	0.006	8.25
thermbias = 0	0.058	0.006	9.16
thermbias = 1	0.053	0.006	8.41
thermbias = 2	0.036	0.006	5.64
thermbias = 3	0.021	0.006	3.35
thermbias = 4	0.013	0.006	2.01
thermbias = 5	0.003	0.006	0.41
log10(CTDiv) x sdSTR = 1	0.023	0.032	0.73
log10(CTDiv) x sdSTR = 2	0.094	0.031	2.98
log10(CTDiv) x sdSTR = 3	0.285	0.031	9.15
log10(CTDiv) x sdSTR = 4	0.237	0.031	7.61
log10(CTR) x sdSTR = 1	0.046	0.035	1.31
log10(CTR) x sdSTR = 2	0.113	0.035	3.26
log10(CTR) x sdSTR = 3	0.056	0.035	1.59
log10(CTR) x sdSTR = 4	-0.004	0.037	-0.11

Model Z2, Adjusted  $R^2 = 0.9907$ . Trimmed Gaussian function

Term	Estimate	Std. Error	t value
Intercept	-1.370	0.007	-200.94
log10(CTDiv)	1.930	0.005	351.15
log10(CTR)	-0.001	0.005	-0.18
thermbias = -4	0.003	0.005	0.53
thermbias = -3	0.000	0.005	-0.09
thermbias = -2	-0.013	0.005	-2.57
thermbias = -1	-0.016	0.005	-3.38
thermbias = 0	-0.004	0.005	-0.90
thermbias = 1	-0.009	0.005	-1.78
thermbias = 2	-0.009	0.005	-1.80
thermbias = 3	-0.008	0.005	-1.65
thermbias = 4	0.001	0.005	0.21
thermbias = 5	-0.004	0.005	-0.81

Model Z3, Adjusted  $R^2 = 0.6681$ . Gamma abundance-temperature function

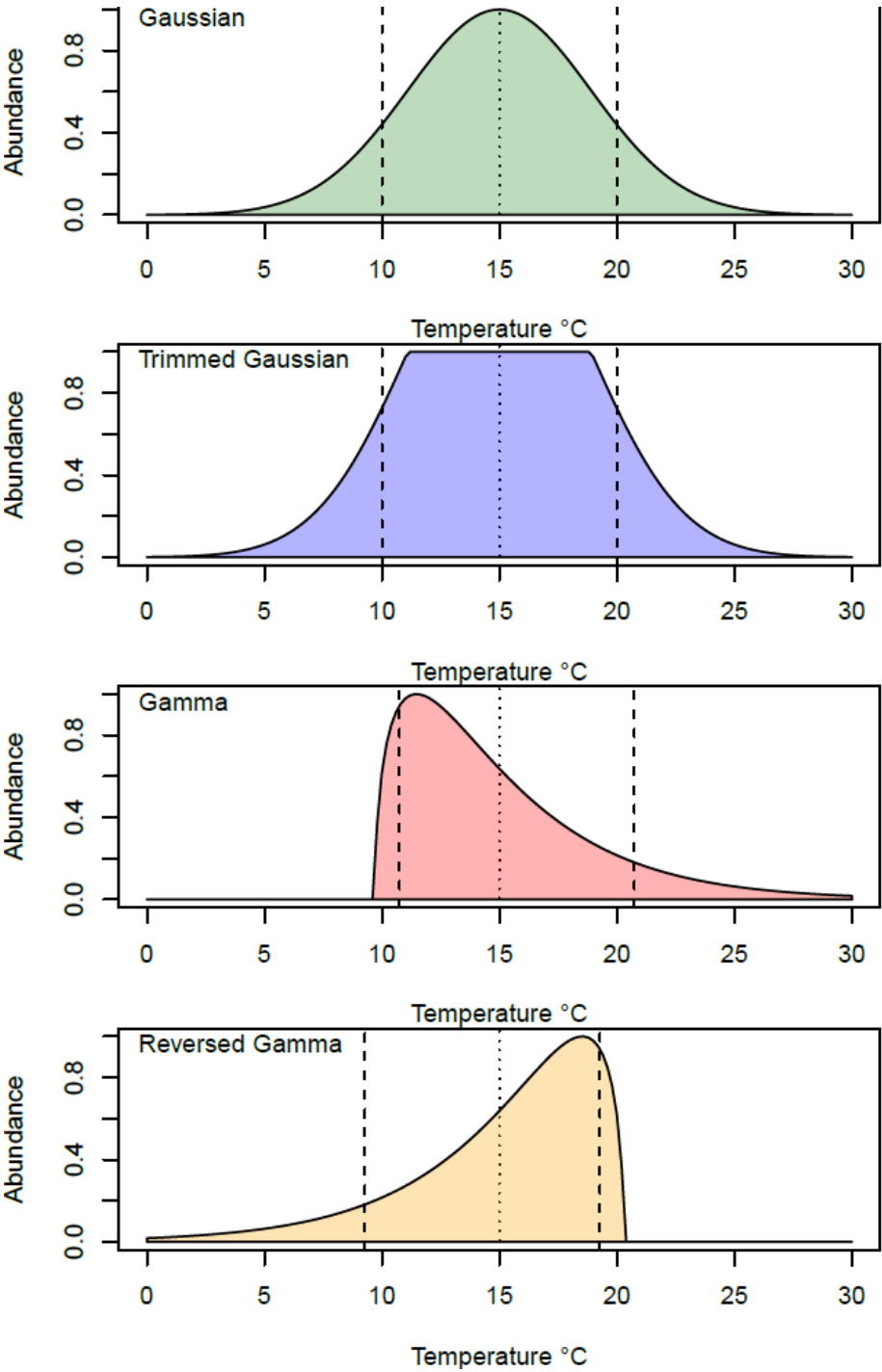
Term	Estimate	Std. Error	t value
Intercept	0.213	0.040	5.34
log10(CTDiv)	0.974	0.048	20.40
log10(CTR)	-1.029	0.054	-19.22
thermbias = -4	0.025	0.016	1.58
thermbias = -3	0.053	0.016	3.31
thermbias = -2	0.084	0.016	5.13
thermbias = -1	0.113	0.017	6.64
thermbias = 0	0.145	0.018	8.09
thermbias = 1	0.187	0.019	9.87
thermbias = 2	0.225	0.020	11.25
thermbias = 3	0.270	0.021	12.70
thermbias = 4	0.308	0.023	13.69
thermbias = 5	0.345	0.024	14.43
shape = 2	0.331	0.052	6.35
shape = 3	0.375	0.052	7.16
shape = 4	0.392	0.052	7.47
log10(CTDiv) x shape = 2	0.823	0.064	12.90
log10(CTDiv) x shape = 3	0.912	0.066	13.88
log10(CTDiv) x shape = 4	0.942	0.066	14.20
log10(CTR) x shape = 2	-0.768	0.073	-10.48
log10(CTR) x shape = 3	-0.849	0.074	-11.43
log10(CTR) x shape = 4	-0.879	0.075	-11.76

Model Z4, Adjusted  $R^2 = 0.6818$ : Reversed gamma function

Term	Estimate	Std. Error	t value
Intercept	0.563	0.039	14.53
log10(CTDiv)	0.924	0.047	19.53
log10(CTR)	-1.020	0.052	-19.44
thermbias = -4	-0.036	0.015	-2.39
thermbias = -3	-0.074	0.015	-4.85
thermbias = -2	-0.120	0.016	-7.58
thermbias = -1	-0.151	0.017	-9.12
thermbias = 0	-0.194	0.017	-11.15
thermbias = 1	-0.220	0.018	-11.93
thermbias = 2	-0.264	0.019	-13.54
thermbias = 3	-0.294	0.021	-14.22
thermbias = 4	-0.313	0.022	-14.26
thermbias = 5	-0.346	0.023	-14.88
shape = 2	0.338	0.051	6.67
shape = 3	0.368	0.051	7.23
shape = 4	0.383	0.051	7.50
log10(CTDiv) x shape = 2	0.954	0.064	15.03
log10(CTDiv) x shape = 3	0.995	0.065	15.35
log10(CTDiv) x shape = 4	1.005	0.065	15.38
log10(CTR) x shape = 2	-0.834	0.072	-11.61
log10(CTR) x shape = 3	-0.878	0.073	-12.07
log10(CTR) x shape = 4	-0.895	0.073	-12.25

30

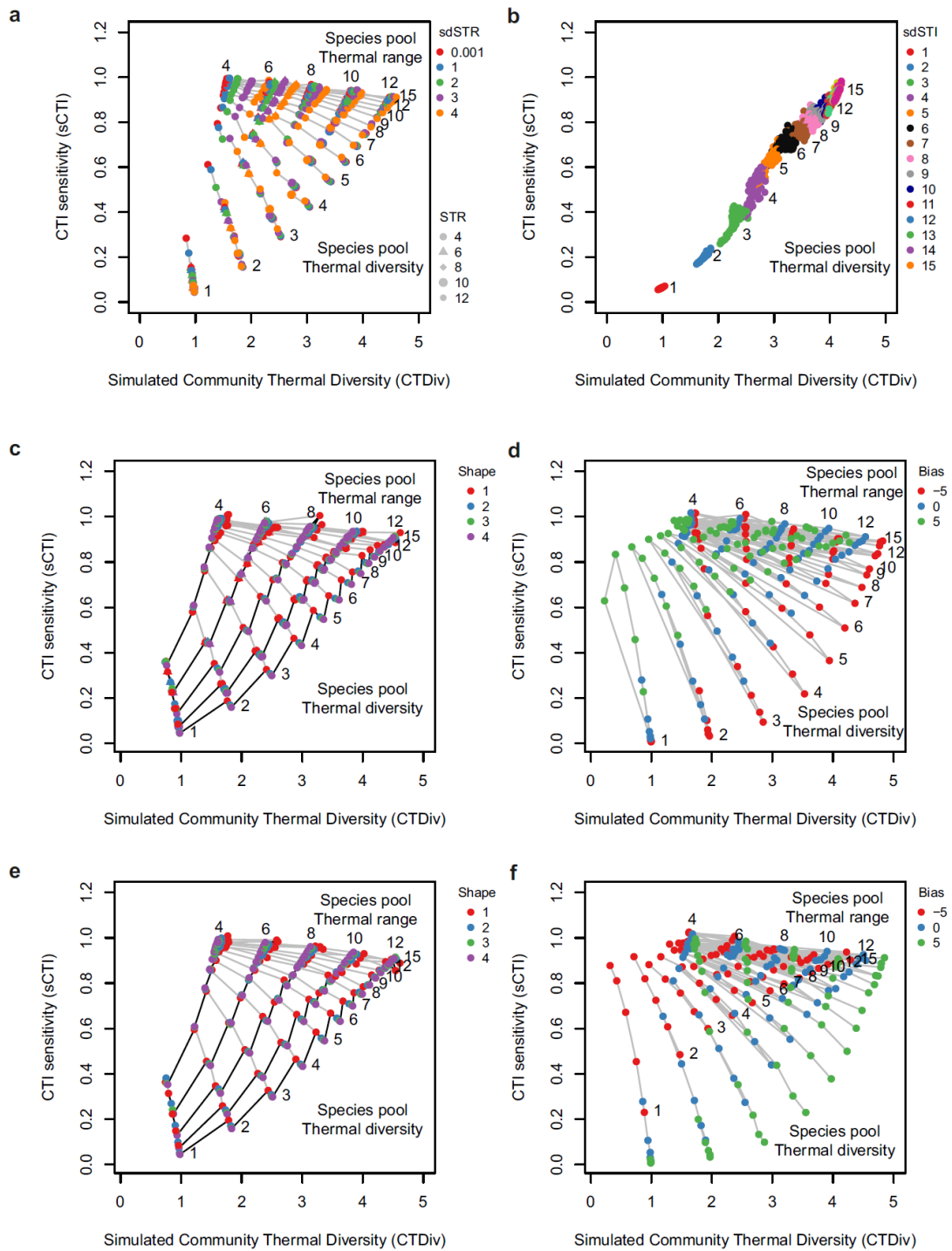
31



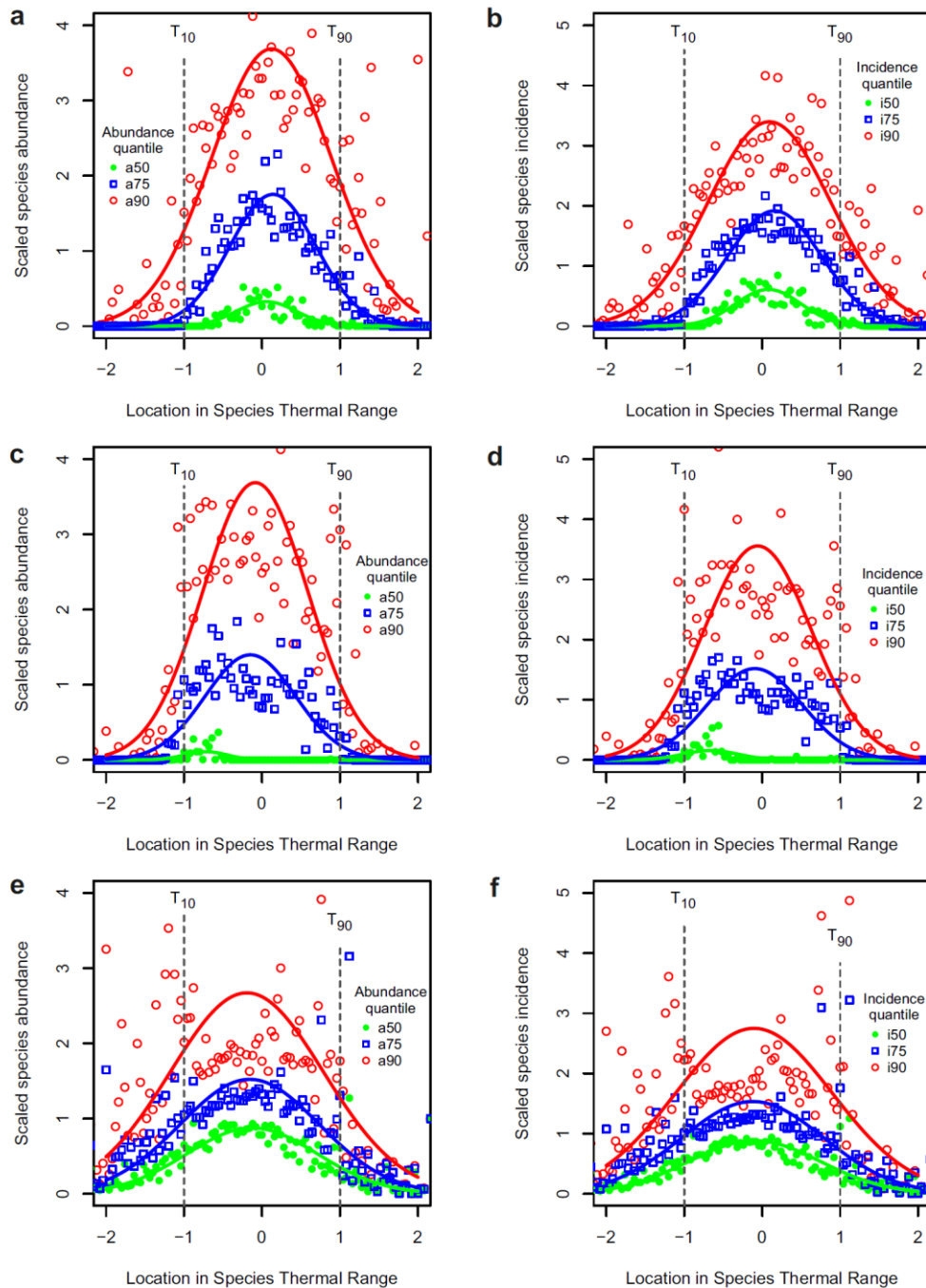
33  
34

35 **Supplementary Fig. 1. | Forms of abundance-temperature relationships used in simulations of**  
36 **CTI sensitivity to changes in temperature: a, Gaussian; b, trimmed Gaussian; c, right-skewed**  
37 **gamma distribution; d, left-skewed gamma distribution. Curves are shown for STI = 15°C and for STR**  
38 **= 10 using gamma shape = 1.5 for c and d.**



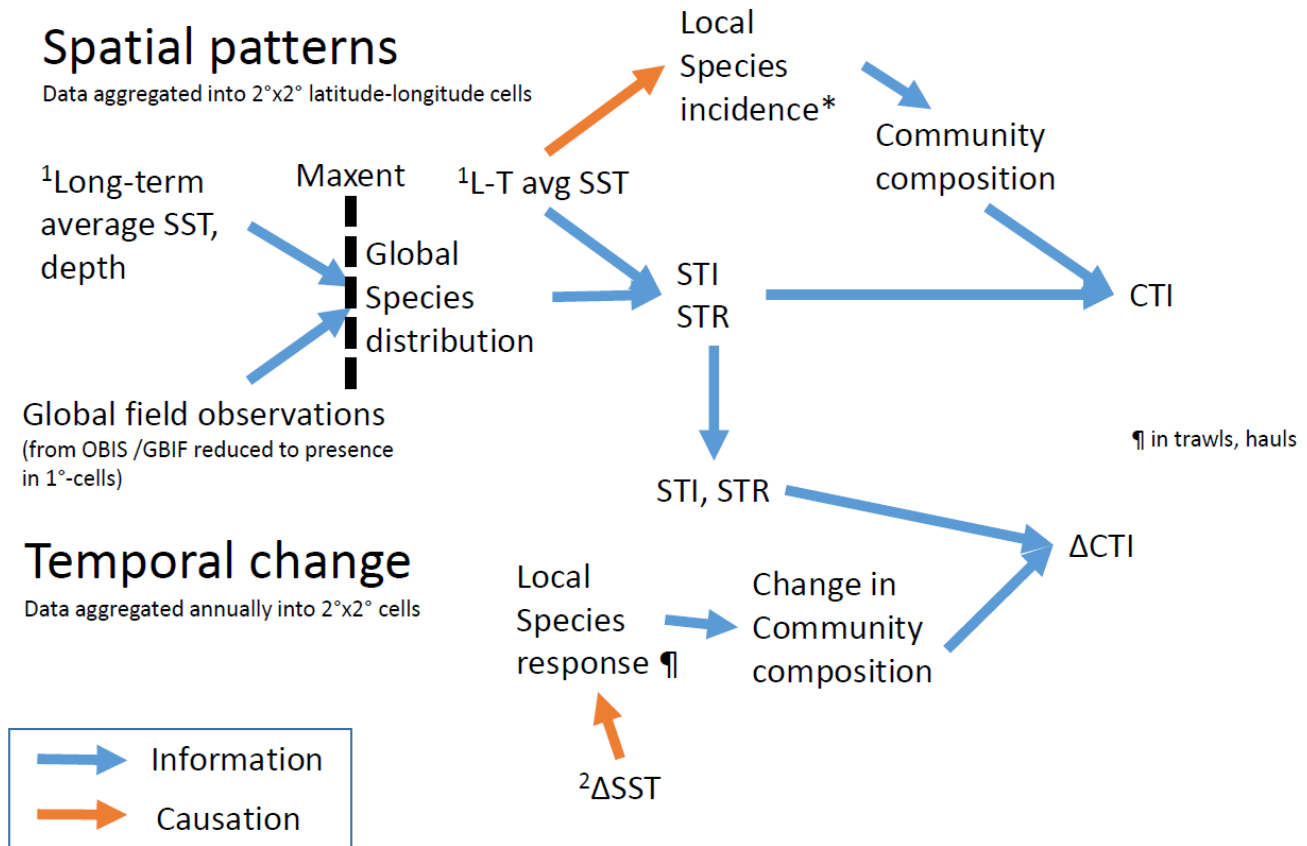


**Supplementary Fig. 2. | Sensitivity of CTI to temperature change in simulated communities. a,** Gaussian abundance-temperature function with varying species range widths; **b,** trimmed Gaussian abundance-temperature function; **c,** gamma function, varying with shape parameter; **d,** gamma function, varying with thermal bias; **e, f,** as **c, d** with the reversed gamma function.



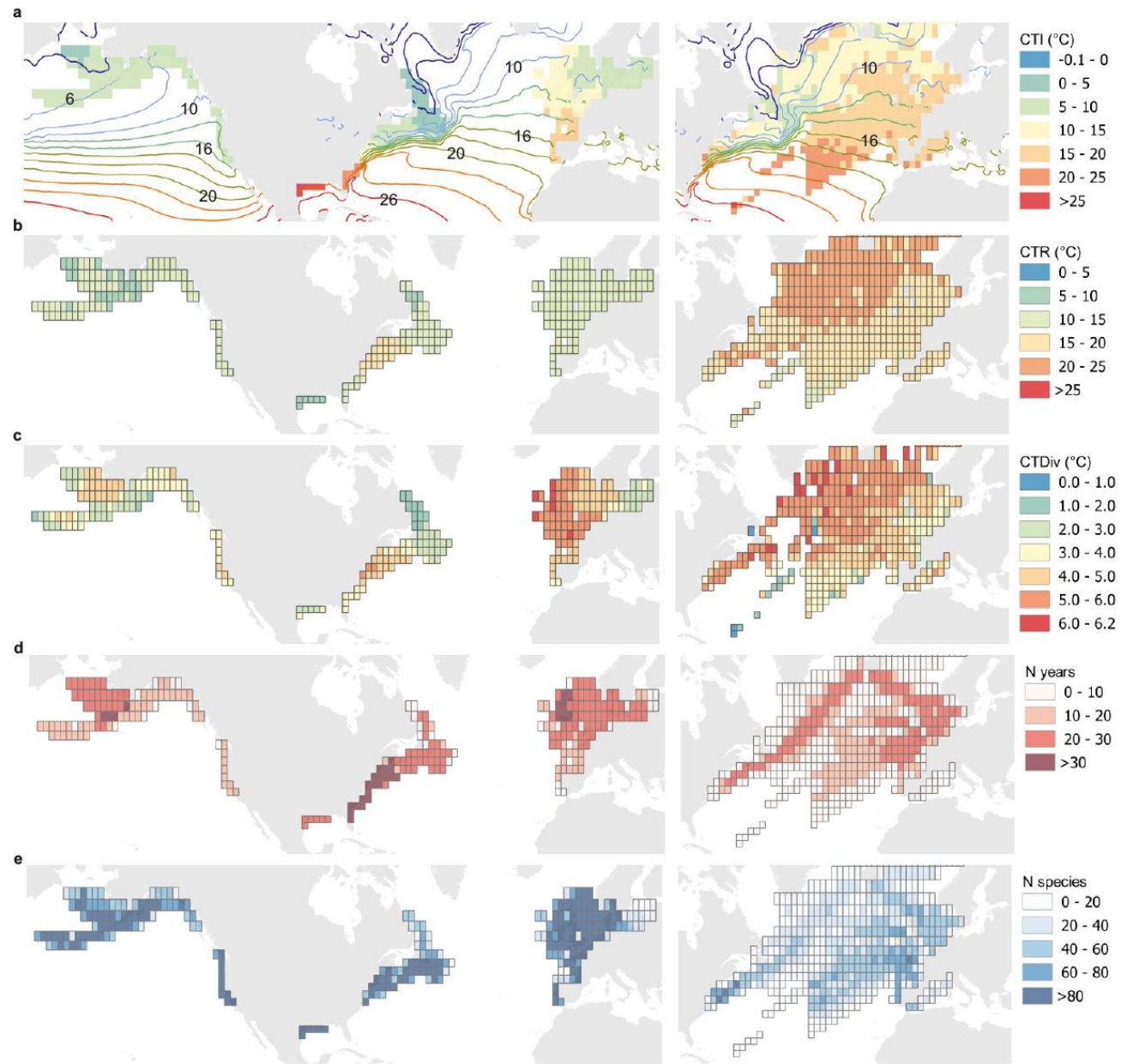
**Supplementary Fig. 3. | Abundance and incidence across scaled locations in species thermal ranges.** Symbols give averages and lines show Gaussian expectations for quantiles (50, 75 and 90th percentiles) of species abundance (**a, c, e**) and incidence (**b, d, f**) in range location classes, after scaling to average values between Species Thermal Range locations -1 ( $T_{10}$ ) to +1 ( $T_{90}$ ), the 10th and 90th percentiles of temperatures occupied in predicted global distribution maps. **a, b**, NMFS species; **c, d**, IBTS species, and **e, f**, CPR species. Red symbols, for example, show how the 90th percentile of all species abundance or incidence values change across from the cold to the warm part of the species thermal range.

\*in trawls, hauls

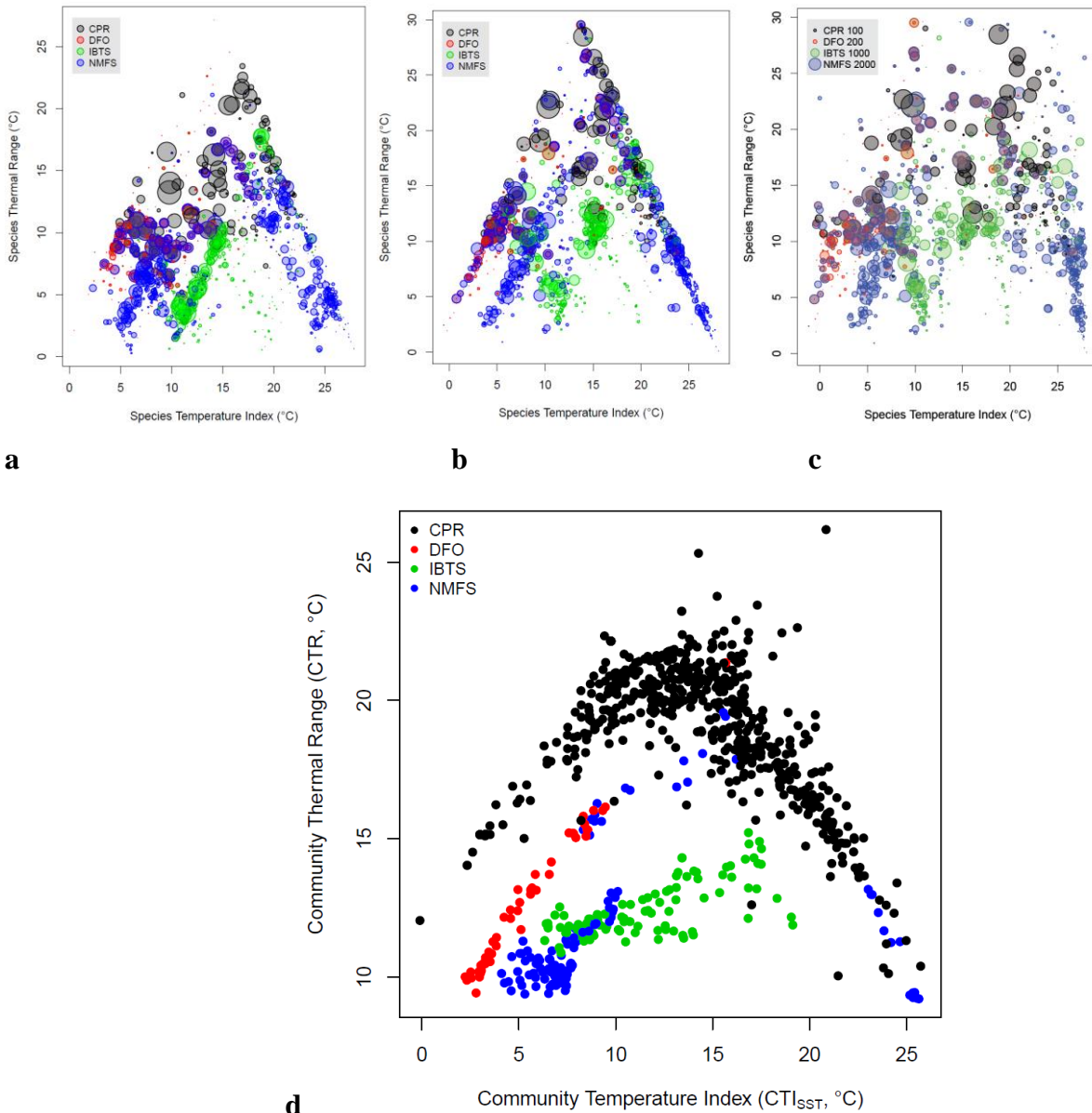


1. SST: Hadley Centre HadISST 1960-2009 average
2. ΔSST: Change in Annual average HadISST

**Supplementary Fig. 4 | Information flow and causation in spatial patterns and temporal trends in Community Temperature Index.** Species thermal affinities (Species Temperature Index values STIs, and Species Thermal Ranges STRs) were derived from the match between global species distributions from global biodiversity data (OBIS) and long-term average temperatures (L-T avg SST). CTI values for bottom trawls and plankton hauls aggregated for 2x2° areas result from the local incidence of species as a response to average temperature. Trends in CTI values over time in these aggregated areas were related to trends in local temperature, taking STIs and STRs from the spatial matching process, but using independent information on change in community composition and temperature change.

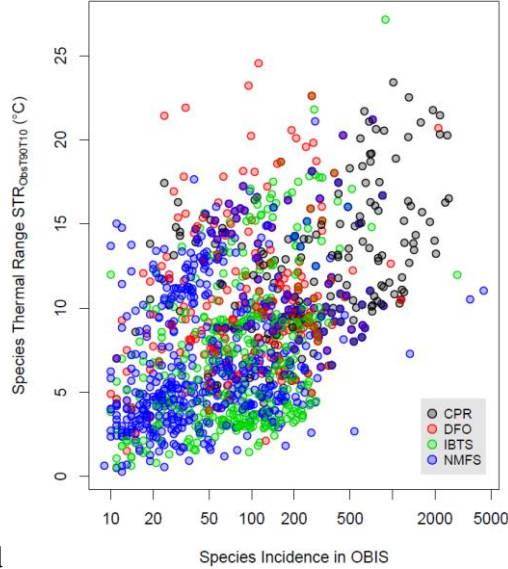
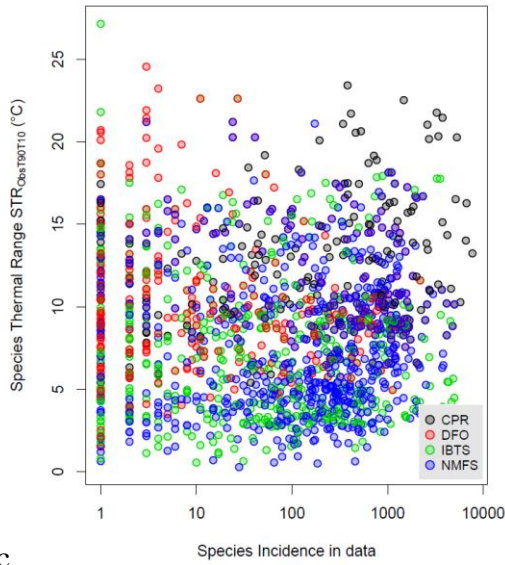
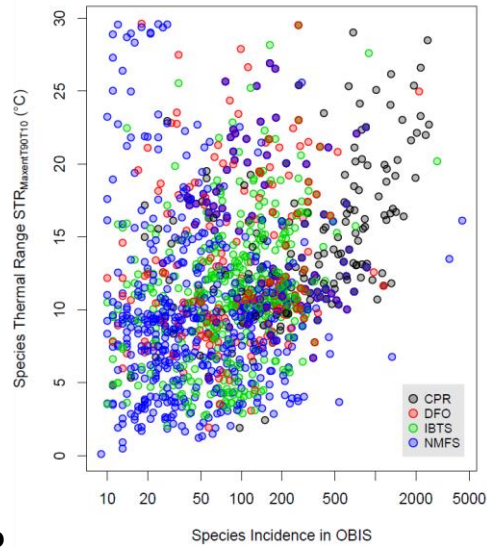
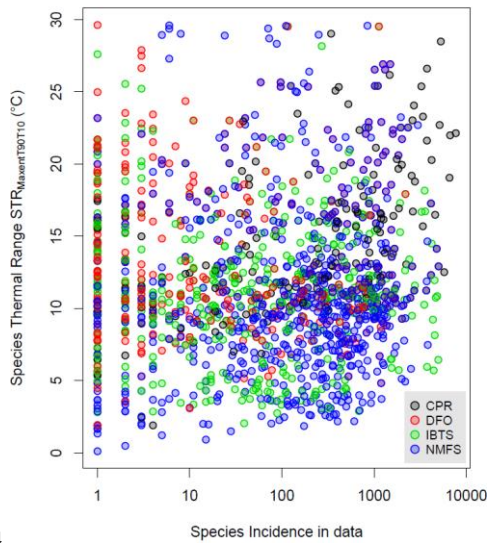


68 **Supplementary Fig. 5 | Spatial patterns in community thermal metrics, duration and number of**  
69 **species recorded in 2° x 2° grid cells in North American and European bottom-trawl surveys (DFO,**  
70 **IBTS, NMFS) and North Atlantic Continuous Plankton Recorder (CPR) surveys. a** Community  
71 **Temperature Index (CTI<sub>SST</sub>) with mean SST as isotherms at 2°C intervals. b** Community Thermal  
72 **Diversity (CTDiv) values. c** Community Thermal Range (CTR). **d**, Number of years sampled. **e**,  
73 **Number of species recorded.**

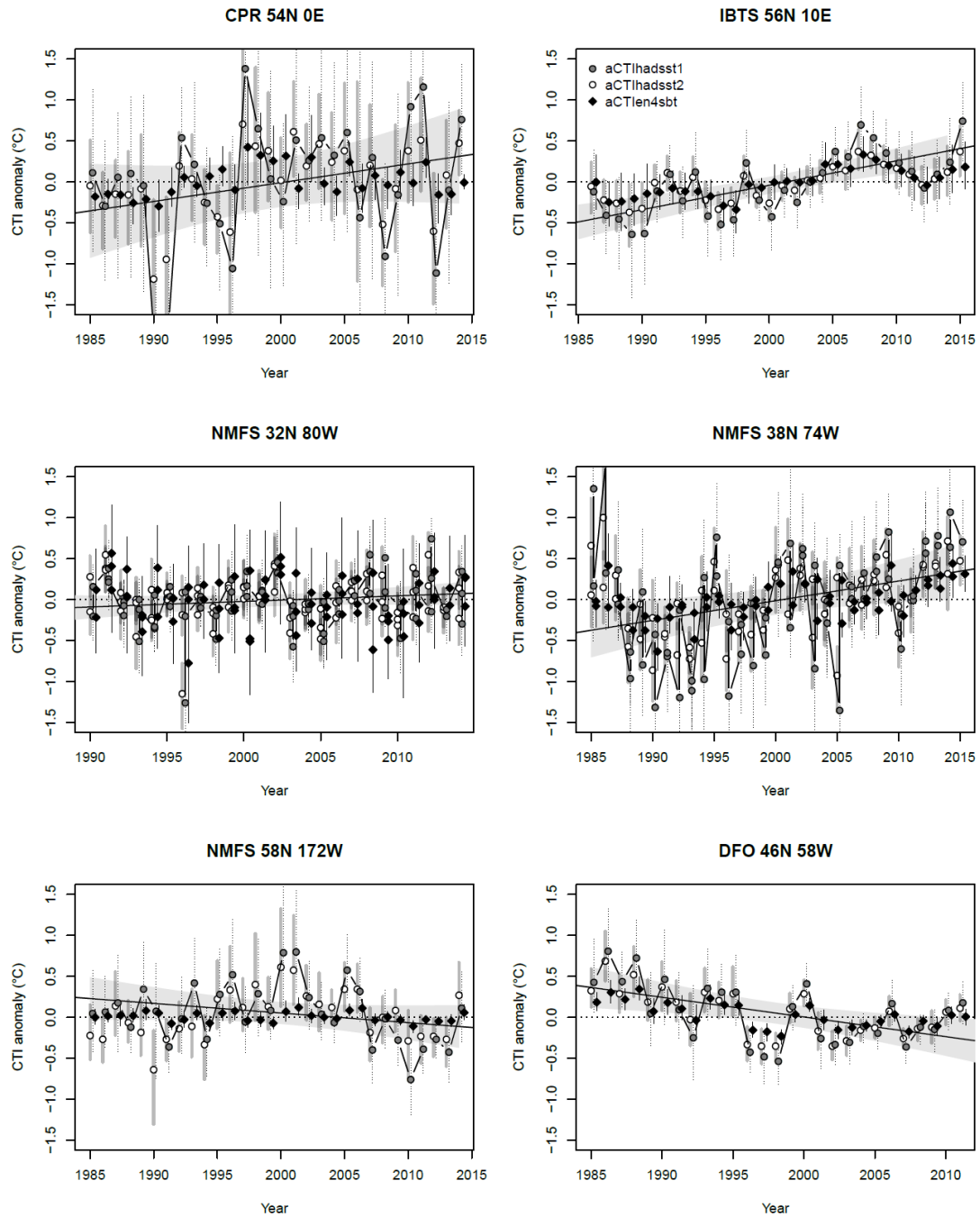


**Supplementary Fig. 6. | Species Thermal Ranges are smaller towards upper and lower bounds of Species Temperature Index but range width is unrelated to species rarity.** Interrelationships among alternate measures of Species Thermal Range (STR) and Species Temperature Index (STI) for species in North American and European bottom-trawl surveys (DFO, IBTS, NMFS) and North Atlantic Continuous Plankton Recorder (CPR) surveys. Metrics were derived by matching average annual Hadley Centre HadISST sea surface temperature (1985 to 2014) to: **a** observation of species presence in OBIS thinned to presence in 1° grid cells (used for CTI<sub>hadisst2</sub>); **b**, **c** predicted presence in 1-dg cells from Maxent models fitted to OBIS data. Species Thermal Range was calculated as T90 – T10, and Species Temperature Index in **a**, **b** as  $0.5 \times (T90 + T10)$  and as T50 in **c** (used for CTI<sub>hadisst1</sub>). Symbol size indicates the frequency of each species in the combined dataset of bottom trawls and plankton hauls. **d**, Resulting patterns of average species thermal metrics in 2° × 2° areas. Average species thermal range width (Community Thermal Range, CTR) showed a hump-shaped relationship with CTI.

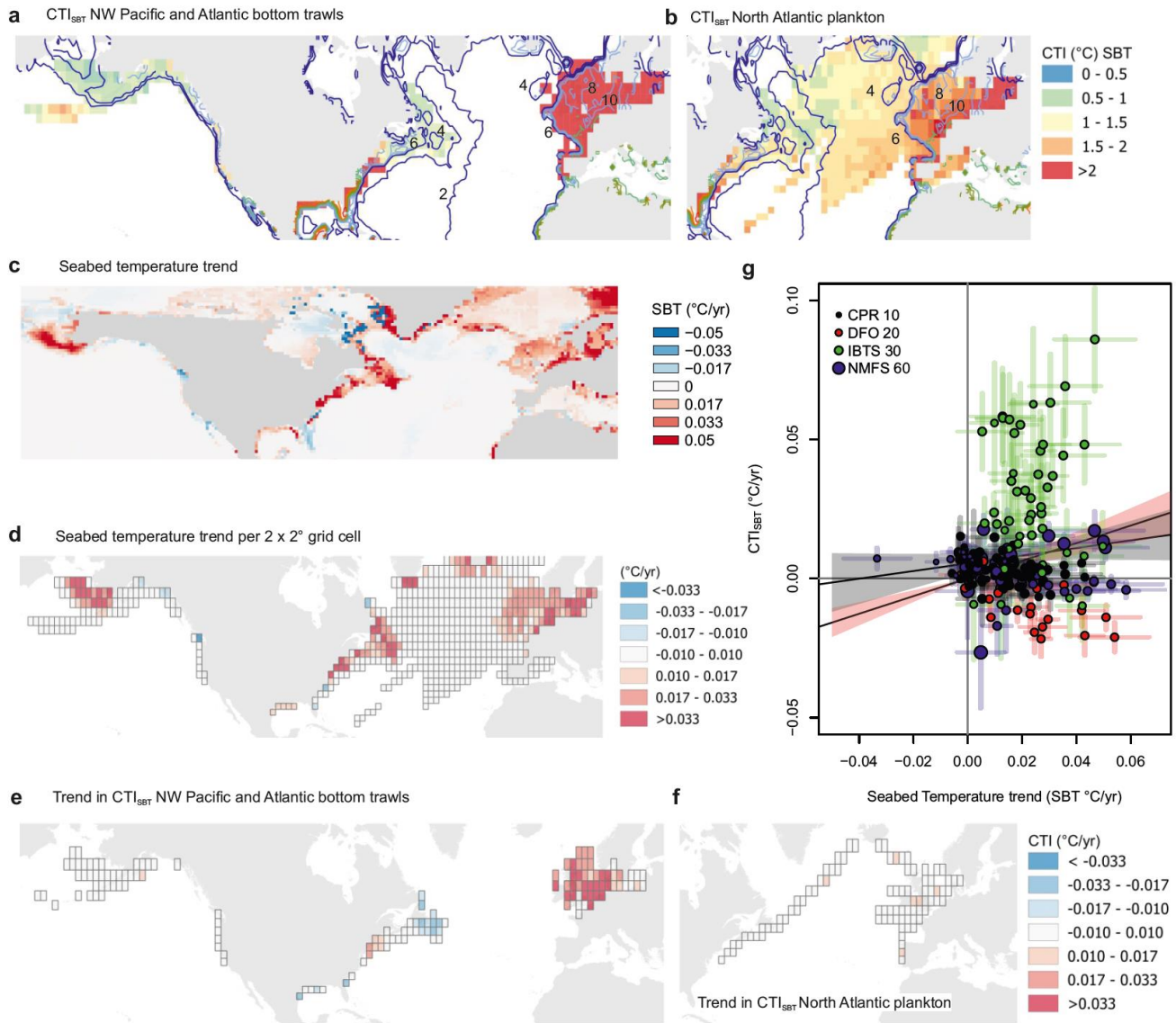




**Supplementary Fig. 7. | Estimated Species Thermal Ranges are not related to species incidence in analysed data but are positively influenced by incidence in a global biodiversity database (OBIS).** Species Thermal Range (STR, T90-T10) derived (a, b) from Maxent models and (c, d) observed presence in 1-dg grid cells plotted against their incidence in (a, c) combined data for bottom trawls and plankton, and (b, d) as presence in 1-dg cells occupied in OBIS data. Species in North American and European bottom-trawl surveys (DFO, IBTS, NMFS) and North Atlantic Continuous Plankton Recorder (CPR) surveys. Incidence in the OBIS dataset had a more marked effect on estimated species thermal range based solely on observations than on STR estimated from Maxent models fitted to these same observations.

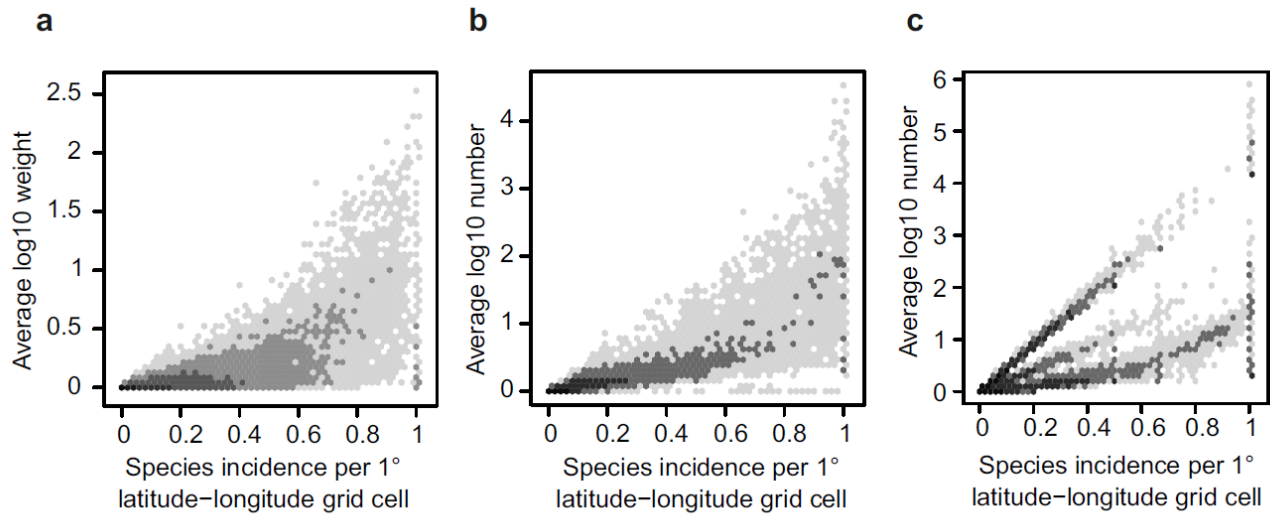


**Supplementary Fig. 8 | Examples of changes from 1985 to 2014 in composition of selected demersal and plankton communities shown by Community Temperature Index (CTI<sub>SST</sub> and CTI<sub>SBT</sub>). Values shown are bootstrapped averages (n=500) of CTI annual anomalies in 2 x 2° latitude-longitude cells. CTIs are based on Species Temperature Index values derived from matching Maxent-modelled distributions to HadISST (aCTI<sub>hadsst1</sub>) and EN4 seabed temperatures (aCTI<sub>en4sbt</sub>), and from the midpoint of extreme observations of species presence in global datasets (aCTI<sub>hadsst2</sub>). Error bars show bootstrap 95% confidence intervals. Solid lines show CTI (aCTI<sub>hadsst1</sub>) regression slopes with shaded 95% confidence intervals.**



**Supplementary Fig. 9 | Patterns of average species thermal affinity and changes in demersal and plankton communities shown by seabed-temperature-derived Community Temperature Index (CTI<sub>SBT</sub>) values from 1985 to 2014, related to seabed temperature trends. a** Spatial patterns in CTI<sub>SBT</sub> with 2°C isotherms showing average seabed temperature (SBT from the Hadley Centre EN4 Temperature dataset). **c, d**, Trend in seabed temperature (SBT) per 1° and sampled 2x2° aggregated grid cells. **e**, Trends in CTI<sub>SBT</sub> for bottom-trawl communities, and **f**, for Continuous Plankton Recorder communities. **g**, CTI<sub>SBT</sub> trends vs SBT trends. Regression slopes are shown by solid lines  $\pm$  95% confidence intervals for a model with an intercept term (solid line with grey shading,  $R^2 = 0.10$ ), and without an intercept (line with red shading, Model A Supplementary Table 4).





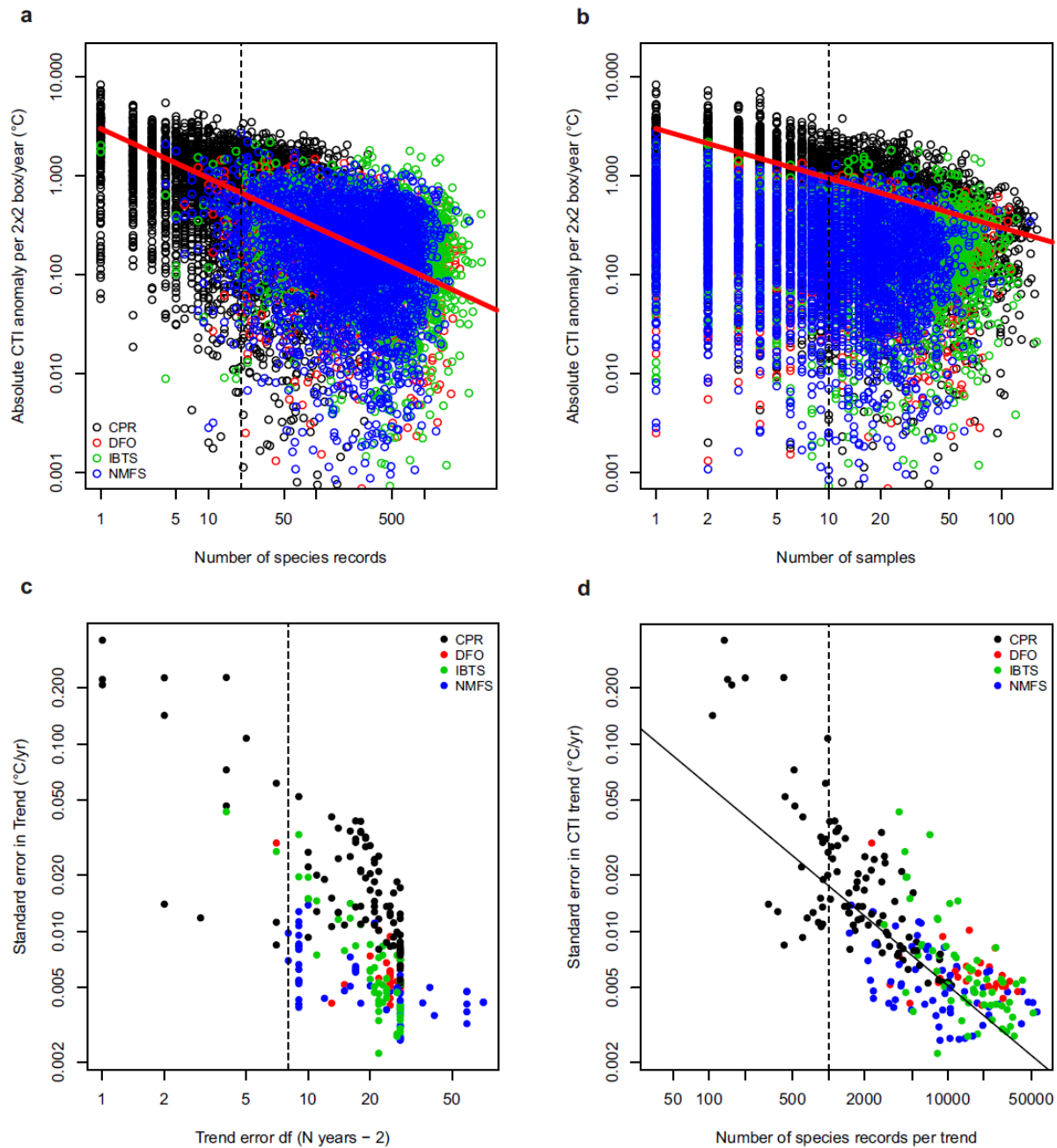
127

128

129 **Supplementary Fig. 10 | Average abundance versus relative frequency of occurrence (incidence)**  
130 **for all species with thermal affinity information in all samples in 1° latitude-longitude cells in a,**  
131 **CPR data; b, IBTS data; and c, NMFS data. Data are shown as frequencies in hexagonal bins, with**  
132 **darker shades showing higher frequencies.**

133

134



135

136

137

138

139

140

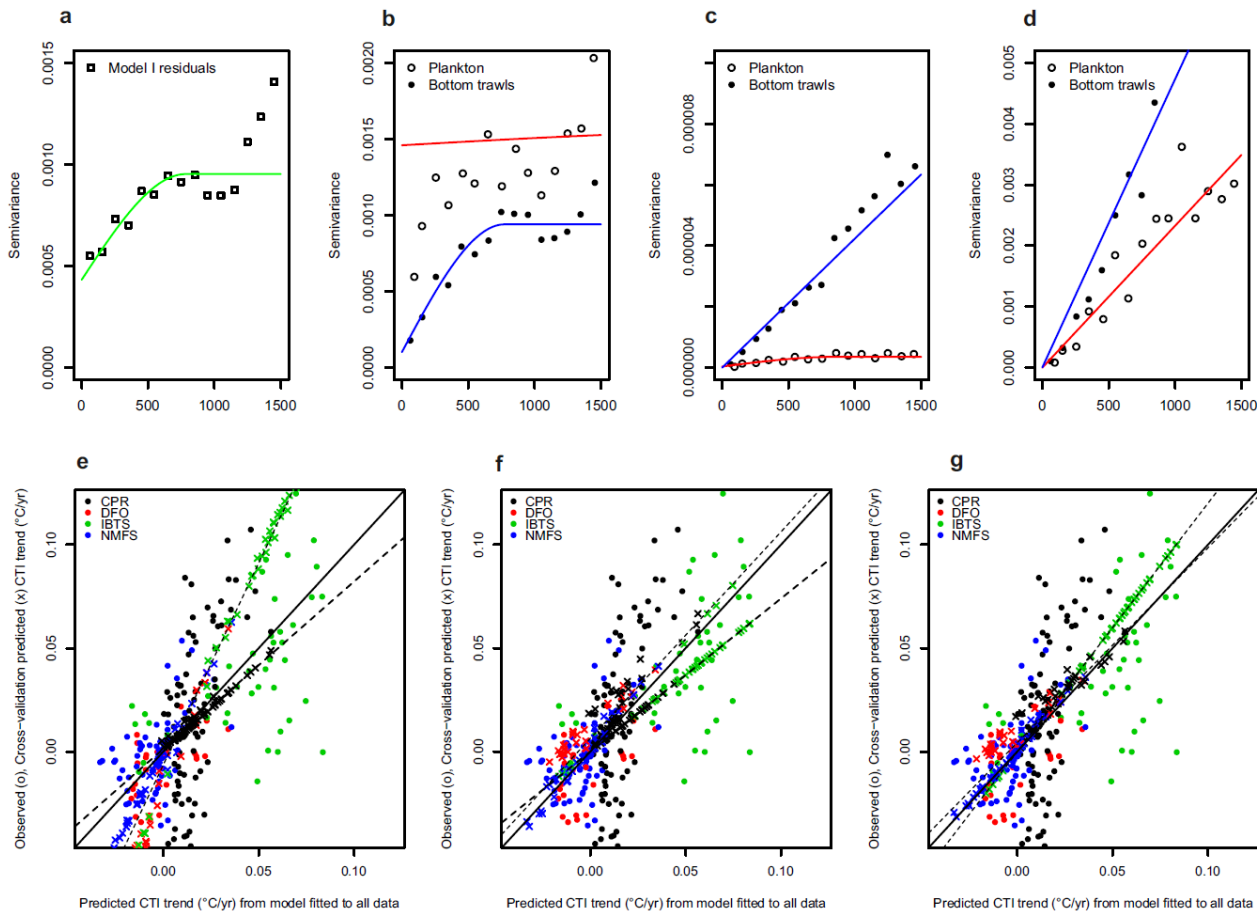
141

142

143

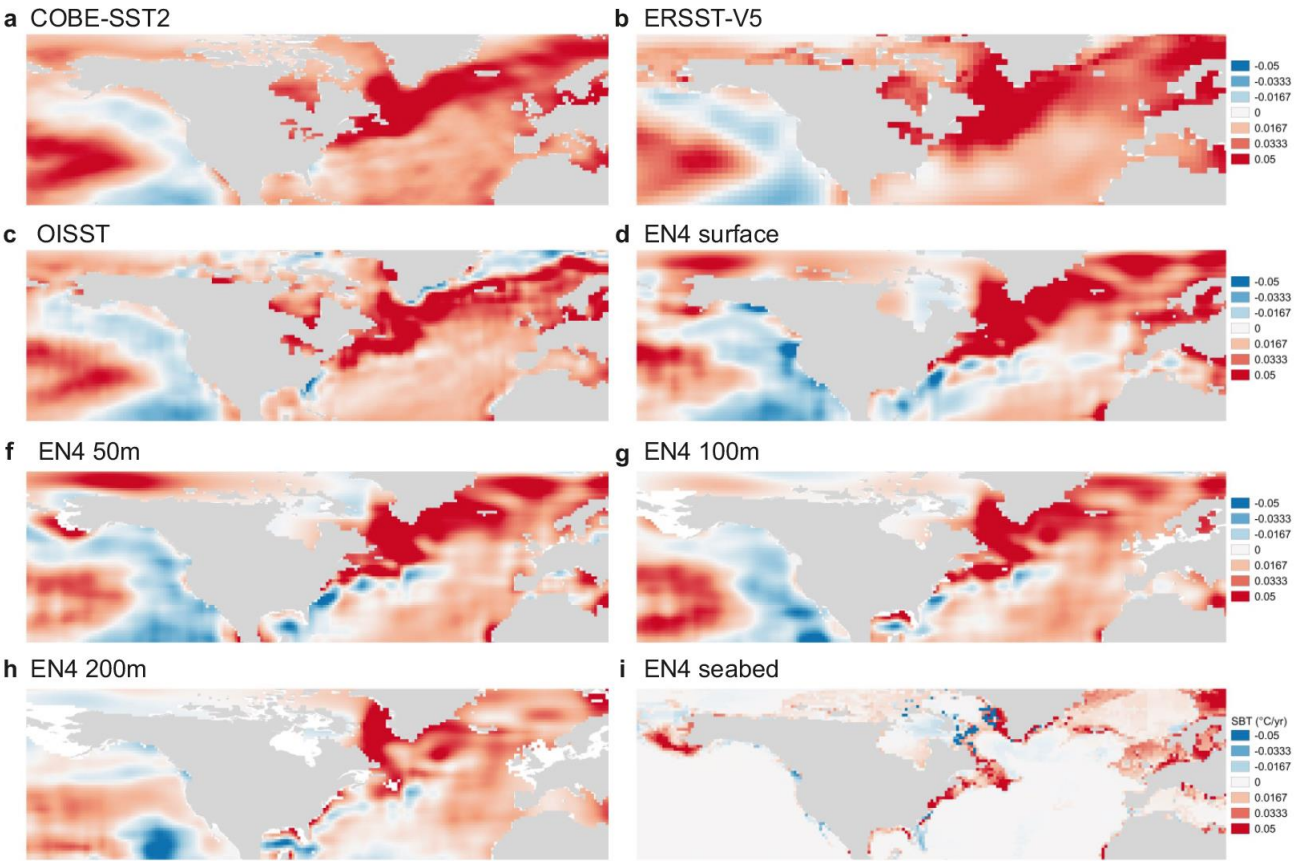
**Supplementary Fig. 11. | Uncertainty in annual means and trends in CTI<sub>SST</sub> in 2° x 2° grid cells shown by the magnitude of anomalies from 1985 to 2014 means. **a**, CTI<sub>SST</sub> anomaly versus the number of species records making up each annual mean. **b**, CTI<sub>SST</sub> anomaly versus number of bottom trawls and plankton hauls for annual means. Red lines in **a** and **b** show slopes of  $y=x^{-0.5}$ . **c**, Standard error in CTI<sub>SST</sub> trend versus (c) trend error df and (d) number of species records per trend. Vertical dashed lines show filter values: annual CTI anomalies were omitted from trend analysis if made up of (a) less than 20 species records or (b) 10 samples. CTI<sub>SST</sub> trend values were omitted from further analysis if based on (c) <10 years of data or <1000 species occurrence records.**

144  
145



146  
147

148 **Supplementary Fig. 12. | Regression model validation.** Variograms showing the spatial error  
149 structure for: **a**, residuals from Model I; **b**, CTI trends data; and **c**, **d**: predictor variables derived from **c**  
150 temperature trends and community thermal composition metrics ( $ST\ trend \times CTDiv^2/CTR^2$ ); and **d**,  
151 temperature trends and vertical temperature gradients ( $ST\ trend \times sless50m$ ). Plots **e**, **f**, **g** show plots of  
152 observed CTI trends versus predicted CTI trends, using subsets as training and test data: **e**, split by  
153 plankton and bottom trawls; **f**, split by latitude, and **g** by longitude. Crosses in **f**, **g**, **h** show predictions  
154 for test data from models fitted to training sets.



158 **Supplementary Fig. 13. | Trends from 1985 to 2014 in different Sea Temperature (ST) measures.**



162  
163  
164  
165  
166  
167  
168  
169